

Accepted Manuscript

Title: 5-Hydroxymethylfurfural Catalytic Oxidation Under Mild Conditions by Co (II), Fe (III) And Cu (II) Salen Complexes Supported on SBA-15: Synthesis, Characterization and Activity

Authors: Daniela Xulú Martínez-Vargas, Javier Rivera De La Rosa, Ladislao Sandoval-Rangel, Jorge Luis Guzmán-Mar, Marco A. Garza-Navarro, Carlos J. Lucio-Ortiz, David A. De Haro-Del Río

PII: S0926-860X(17)30416-7
DOI: <http://dx.doi.org/10.1016/j.apcata.2017.08.035>
Reference: APCATA 16390

To appear in: *Applied Catalysis A: General*

Received date: 11-8-2017
Accepted date: 21-8-2017

Please cite this article as: Daniela Xulú Martínez-Vargas, Javier Rivera De La Rosa, Ladislao Sandoval-Rangel, Jorge Luis Guzmán-Mar, Marco A. Garza-Navarro, Carlos J. Lucio-Ortiz, David A. De Haro-Del Río, 5-Hydroxymethylfurfural Catalytic Oxidation Under Mild Conditions by Co (II), Fe (III) And Cu (II) Salen Complexes Supported on SBA-15: Synthesis, Characterization and Activity, *Applied Catalysis A, General* <http://dx.doi.org/10.1016/j.apcata.2017.08.035>

This is a PDF file of an unedited manuscript that has been accepted for publication. As a service to our customers we are providing this early version of the manuscript. The manuscript will undergo copyediting, typesetting, and review of the resulting proof before it is published in its final form. Please note that during the production process errors may be discovered which could affect the content, and all legal disclaimers that apply to the journal pertain.



5-Hydroxymethylfurfural Catalytic Oxidation Under Mild Conditions by Co (II), Fe (III) And Cu (II) Salen Complexes Supported on SBA-15: Synthesis, Characterization and Activity

Daniela Xulú Martínez-Vargas¹, Javier Rivera De La Rosa^{*1,2}, Ladislao Sandoval-Rangel¹, Jorge Luis Guzmán-Mar¹, Marco A. Garza-Navarro^{2,3}, Carlos J. Lucio-Ortiz¹ and David A. De Haro-Del Río¹

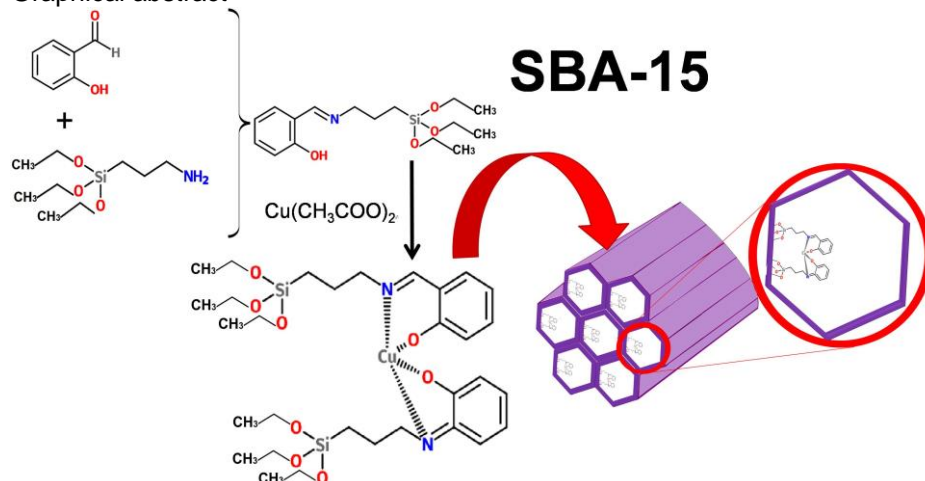
¹Universidad Autónoma de Nuevo León, UANL, Facultad de Ciencias Químicas, Ave. Universidad S/N, Cd. Universitaria, San Nicolás de los Garza, N. L., C.P. 64451, México. Tel.: +528180294000 ext 6357; fax: +52818029400 ext 6282.

²Universidad Autónoma de Nuevo León, UANL, Centro de Innovación, Investigación y Desarrollo en Ingeniería y Tecnología (CIIDIT), Km 10 de la nueva carretera al Aeropuerto Internacional de Monterrey, PIIT Monterrey, 66600, Apodaca, Nuevo León, México.

³Universidad Autónoma de Nuevo León (UANL), Facultad de Ingeniería Mecánica y Eléctrica (FIME), Av. Universidad S/N, Cd. Universitaria, San Nicolás de los Garza, Nuevo León C.P. 66451, México

Corresponding author: *javier.riverad@uanl.edu.mx

Graphical abstract



Highlights

- Synergistic effect of Cu (II) and Fe(III) Salen catalysts supported on SBA-15 and H_2O_2 in HMF oxidation
- Cu Salen/SBA-15 catalyst active in HMF oxidation under mild conditions
- Mechanism of HMF catalytic oxidation step by step
- Higher selectivity to oxidation of alcohol group compared with the aldehyde group of HMF molecule

ABSTRACT

In the present work, an alternative system of 5-hydroxymethylfurfural (HMF) oxidation was studied, in an effort to avoid the use of expensive precious metal catalysts, high pressures and systems not

environmentally friendly. The catalysts tested were Co (II), Fe (II) and Cu (II) Salen complexes supported on SBA-15 (Co Salen/SBA-15, Fe Salen/SBA-15 and Cu Salen/SBA-15 respectively). The reaction was carried out in aqueous medium at room temperature ($25\text{ }^{\circ}\text{C} \pm 1$) and atmospheric pressure, using hydrogen peroxide (H_2O_2) as the only oxidant agent. The effect of various reaction conditions such as H_2O_2 content, oxidant agent amount, different transition metals present in the catalyst and temperature were evaluated. The HMF and the reaction products such as; 2,5-diformylfuran (DFF), 2,5-furandicarboxylic acid (FDCA), 5-hydroxymethyl-2-furancarboxylic acid (HMFCFA) and 5-formyl-2-furancarboxylic acid (FFCA) were followed by high performance liquid chromatography (HPLC) measurements. The selectivity and reaction kinetics under different reaction conditions was studied. The different synthesized catalysts were extensively characterized by UV-vis spectroscopy, subsequently by FTIR, DR-UV-vis, AA and XPS spectroscopy and through nitrogen physisorption, which was related to its catalytic activity. The successful synthesis of SBA-15 support was confirmed by its textural properties and STEM. From the experimental data obtained a reaction mechanism with parallel reactions was proposed founding that the oxidation route of the alcohol group in HMF is favored over of the oxidation of the aldehyde group on the other side of the molecule.

KEYWORDS

5-hydroxymethylfurfural oxidation, Co(II) Salen SBA-15, Cu (II) Salen SBA-15, Fe (III) Salen SBA-15.

1. INTRODUCTION

During the past decade, one of the global concerns has been the use of fossil fuels for the production of energy and chemicals, due to their limited availability and the pollution caused for their use [1, 2]. Nowadays, the production of both energy and chemicals requires alternative resources and a more severe environmental control [2, 3]. Therefore, biomass sources are the most promising alternative for the replacement of fossil resources, due to their abundance in nature and low cost. About 75% of naturally available biomass is composed of carbohydrates, then, much interest has been given to the development of efficient approaches to transform carbohydrates,

derived from biomass, into value-added chemicals [4, 5]. However, the use of biomass has caused considerable controversy due to ethical issues, employing the use of edible products for biomass such as corn and sugar cane, which are used as raw materials in bioethanol production [1, 6]. Due to these precedents, research is being directed to the use of biomasses derived from agroindustrial waste, uncultivable or inedible raw materials.

Catalytic oxidation, either homogeneous or heterogeneous is a very powerful tool in the synthesis of fine chemicals [7, 8]. In such synthesis, compounds derived from furfural which have functional groups in position five have played an important role [1]. Therefore, the 5-hydroxymethylfurfural (HMF) is considered an important and versatile platform precursor for the synthesis of this kind of compounds with applications in pharmaceutical and polymers industry, whose syntheses are attempted from carbohydrates such as fructose, glucose, cellulose, etc. [2, 9-14]. HMF oxidation leads to the formation of different products such as 5-hydroxymethyl-2-furancarboxylic acid (HMFA), 2,5-diformylfuran (DFF), 5-formyl-2-furancarboxylic acid (FFCA) and 2,5-furandicarboxylic acid (FDCA) [7, 15]. FDCA is a promising biomass-derived chemical building block with a great market potential, due to being considered as a monomer for synthesis of a new polymer class, and also as a potential replacement of terephthalic acid, mainly used as precursor in the production of polyethyleneterephthalate (PET) [1, 2, 16, 17]. DFF is considered as a highly useful chemical with applications in pharmaceuticals, fungicides, organic conductors and macrocyclic ligands [7, 18-21]. It has attracted great attention as a monomer in the production of multifunctional polymeric materials with special applications [22-26]. HMFA and FFCA are intermediary products. At the same time, the oxidative cleavage of the furan ring of HMF could take place; resulting in the formation of succinic acid, 2-oxoglutaric acid, maleic acid and fumaric acid [27, 28]. Levulinic acid and formic acid could also be present due to HMF hydration in the presence of an acid catalyst [28, 29]. The classical synthesis of FDCA and DFF from HMF usually involves high pressure and temperature, metal salts (generally based on noble metals) and organic solvents [7, 30], which makes the process expensive and polluting [2, 31-33].

The use of expensive, noble metal-based catalysts such as Ru, Pt [34-38], Pd [35, 39-41], Rh and Au [35, 36] in the HMF oxidation has been recently reported; Nie *et al.*[30] studied Ru, Pt, Pd, Rh

and Au [36] catalysts using activated carbon (C), Mg_2AlO_x , MgO, Al_2O_3 , ZSM-5, TiO_2 , ZrO_2 and CeO_2 as supports; they found that the Ru/C catalyst showed the best performance with a DFF yield of 96% at 110°C, high pressure of pure O_2 (2 MPa) and toluene as solvent, known by its toxicity. Antonyraj *et al.* [42] also found a high DFF yield of 97% with a 99% conversion of HMF employing Ru/ γ - Al_2O_3 and toluene as a solvent with 0.28 MPa of pure oxygen. Although other catalysts such as VO^{2+}/Cu^{2+} on sulfonated carbon [7], copper complexes [43, 44], Mn (III) Salen complex [45] and gold nanoparticles on hydrotalcite have also been studied and shown high selectivity to DFF or FDCA, most of them have serious disadvantages such as being expensive and/or homogeneous, in the presence of unfavorable conditions like organic solvents, high pressures, promoters and different oxidizing agents (sometimes using more than one at a time). Vanadium species are known for their toxicity and also oxidizing agents such as chromate (CrO_4^{2-}), dichromate ($Cr_2O_7^{2-}$) and permanganate (MnO_4^-), that have been often employed to oxidize HMF [44]. Therefore, it is still necessary to improve processes through non-expensive and readily available catalysts, which can operate at more favorable conditions such as low pressure and temperature (which will decrease costs and will make the processes safer and simpler) in addition to a decreased use of solvents and harmful materials to health and the environment in the reaction system.

In the present study, HMF oxidation was investigated under mild conditions such as aqueous media with H_2O_2 , which is considered as environmentally friendly and green oxidation reagent, with metal (Co (II), Cu (II) and Fe (III)) Salen complex catalysts supported on SBA-15 (Co Salen/SBA-15, Cu Salen/SBA-15 and Fe Salen/SBA-15) as a first study of this system as an alternative for the synthesis of compounds of high added value, a system which has not been previously studied. Salen metal complexes can be used to simulate the catalytic behavior of an enzyme [44], which makes them attractive for their use in catalysis, although they have been used mainly in homogeneous reaction systems. An extensive characterization of the heterogeneous catalysts synthesized is reported in this work, also the effect of different conditions in the HMF reaction system and a reaction mechanism is proposed.

2. EXPERIMENTAL

2.1 Materials and methods.

Pluronic P123 and tetraethyl orthosilicate (TEOS) were used to synthesize SBA-15. Salicylaldehyde (99%) and 3-aminopropyltriethoxysilane (99%) from Aldrich (St. Louis, MO, USA) was used for the ligand synthesis and the cobalt (II) acetate tetrahydrate (>98%) and copper (II) acetate (98%) from Aldrich (St. Louis, MO, USA) and iron (III) chloride hexahydrate (>99%) from Desarrollo de Especialidades Químicas (San Nicolás de los Garza, N.L., México) as metallic precursors for the formation of the respective metal Salen complex. Methanol (ACS Reagent 99.8%) from JT Baker (Central Valley, PA, USA) was used as a solvent. 5-hydroxymethylfurfural \geq 99%, 2,5 diformylfuran (97%), 2,5-furandicarboxaldehyde (97%), 5-formyl-2-furoic acid and 5-hydroxymethyl-2-furancarboxylic acid (Sigma-Aldrich, St. Louis, MO, USA), were used as standards for analytical measures. Nanopure water was used as reaction media (50 mL). Hydrogen peroxide 30 p/V% (CTR Scientific, Monterrey, N.L., México) also was added (50 μ L) before the catalyst was incorporated.

In order to follow the oxidation process, the substrate (HMF) and major products of the expected reaction (2,5 diformylfuran (DFF), 2,5-furandicarboxaldehyde (FDCA), 5-formyl-2-furoic acid (FFCA) and 5-hydroxymethyl-2-furancarboxylic acid (HMFCA)) were separated by High-performance liquid chromatography (HPLC) using the HPLC Perkin Elmer Equipment with UV detector and an Aminex HPX-87H 300 X 7.8 mm column (cross-linked resin hydrogen ionic form, sulfonated divinyl benzene-styrene copolymer as support, 9 μ m particle size) from Bio-Rad (Hercules, California, USA). The mobile phase used was H₂SO₄ 5mM in water. All aqueous solutions were prepared with nanopure water.

The column was conditioned every day before the analyses by flowing the mobile phase through the column (1.2 mL/min) until no peaks or baseline noise were showed in the chromatogram. Following this the sample was manually injected when the display marked 0.2 mL/min, in order to control the migration time (t_M) in each injection. 25 μ L of the sample were consecutively injected three times, in order to have an excess amount and to ensure repetitiveness of the injections. The method used consisted of a 30 min run, a 1.2 mL/min flow and room temperature (25 °C), using the previously described mobile phase. An UV detector was used with $\lambda = 250$ nm. At the end of each

working day, the column was cleaned by flowing the mobile phase. Although this procedure increased the reproducibility, slight shifts in t_m were observed and considered normal.

Sampling was conducted by taking 500 μL of the reaction solution (carried out in deionized water) and centrifuged to remove the catalyst (6000 rpm for 1 min). Data acquisition was performed using the TotalChrom software (Perkin Elmer, Shelton, CT, USA). Each mobile phase solution was prepared daily and degassed by sonication for 15 min before use. The capillary was conditioned with 5 mM of H_2SO_4 at least during 30 min.

2.2 Characterization.

The amount of metal loading (Co, Cu or Fe active site according to the respective metal Salen complex on SBA-15) was quantified by Atomic absorption spectroscopy (AAS) using an AA 1 Thermo Jarrell Ash Scan (Franklin, MA, USA) with a hollow cathode lamp as the light source. For Co analysis the lamp used was No: 62928162928-02, lamp current: 3 mA operating in background Hiefje Smith (the signal is matched to the intensity of the background), λ : 240.7 nm pass band: 0.3 nm, Burnt head: long history, air-acetylene flame. Sensitivity of 0.044 absorbance = 1% absorption about 0.05 $\mu\text{g}/\text{mL}$ for the instrument with the parameters described. The standard of 1.2 $\mu\text{g}/\text{mL}$ Co gives an approximate reading of 0.1 A. Linear range of Co: linear concentration above 5 $\mu\text{g}/\text{mL}$ (aqueous solution using the instrumental parameters described above). For the measurement of Cu the lamp used was No: 63041/63041-02, lamp current: 2.5 mA operating in background Hiefje Smith (the signal is matched to the intensity of the background), λ : 324.7 nm pass band: 1.0 nm, Burnt head: long history, air-acetylene flame. Sensitivity of 0.0044 absorbance = 1% absorption about 0.03 $\mu\text{g}/\text{mL}$. The standard of 0.7 $\mu\text{g}/\text{mL}$ Co gives an approximate reading of 0.1 A. Linear range of Cu: linear concentration above 4 $\mu\text{g}/\text{mL}$ (aqueous solution using the instrumental parameters described above). Finally, for Fe the lamp used was No: 62810/62810-02, lamp current: 3 mA operating in background Hiefje Smith (the signal is matched to the intensity of the background), λ : 248.3 nm pass band: 0.3 nm, Burnt head: long history, air-acetylene flame. Sensitivity of 0.044 absorbance = 1% absorption about 0.04 $\mu\text{g}/\text{mL}$ for the instrument with the parameters described. The standard of 1.0 $\mu\text{g}/\text{mL}$ Fe gives an approximate reading of 0.1 A. Linear

range of Fe: linear concentration above 5 $\mu\text{g} / \text{mL}$ (aqueous solution using the instrumental parameters described above). Fourier-transform infrared (FTIR) spectroscopy was performed using a Nicolet 6700 FTIR spectrometer (Thermo Scientific, Waltham, MA, USA) with KBr disks and also the Sprettrum One FTIR-ATR spectrometer (Perkin-Elmer, Waltham, MA, USA). UV–Vis spectra were measured with a Genesys 10UV scanning (Thermo Electron Corporation, Madison, WI, USA) spectrophotometer, which was operated in the region of 200–800 nm and used quartz cuvettes (Fisher Scientific, Pittsburgh, PA, USA). UV–Vis diffuse reflectance spectra were recorded on a Nicolet Evolution 300 PC UV–Vis spectrophotometer (Thermo Scientific, Waltham, MA, USA). N_2 sorption isotherms of silica SBA-15 were recorded in a BEL SORP mini II (BEL JAPAN INC., Toyonaka-shi, Osaka 561-0807 JAPAN), plotting relative pressure points of 0.05 – 0.99 and 0.99 – 0.030 for adsorption and desorption, respectively. For these analyses, all samples were degassed at 150 °C for 24 hrs. The measurements were performed using ultra high purity (UHP) grade N_2 as the adsorbent gas and liquid N_2 at -196°C as the medium. The Barrett-Joyner-Halenda (BJH) and Brunauer, Emmet and Teller (BET) methods were used to calculate the pore diameter and surface area, respectively. Surface analyses were performed using an X-ray photoelectron spectrometer K-Alpha Thermo Scientific, with X-ray spot of 400 nm and flood gun for charge compensation. Samples were prepared in discs with KBr. Measurements were performed after ion beam etch with argon ion gun (2 keV during 20 s with 20–40nm estimated thickness); with 400 μm spot size, 50.0 eV pass energy and energy step size of 0.100 eV. The Shirley method was used to estimation of the background signals in XPS spectra. For all samples the C1s was taken as reference (284.83 eV).

2.3 Preparation of metal Salen catalysts.

All catalysts were prepared using a procedure previously reported by Rajabi et al. [46, 47] and modified according to previous reports [8] an schematic representation can be seen in Fig 1. First, 0.217 g (2 mmol) of salicylaldehyde was dissolved in 200 mL of absolute methanol and mixed with 0.473 g (2 mmol) of 3-aminopropyltriethoxysilane (APTES), upon which the solution immediately turned yellow. After stirring for 3 h, the metal precursor was added; 0.254 g (1 mmol) of Co

(CH₃COO)₂·4H₂O, 0.185 g (1 mmol) of Cu(CH₃COO)₂ and 0.271 g (1 mmol) FeCl₃·6H₂O per each catalyst. Further, the solution was stirred for 3 additional hours until its color changed to green for Co and Cu Salen complexes or purple for Fe Salen complex. Next, 3 g of the solid support (SBA-15) were added and kept under stirring overnight (~15 h). Finally, the obtained solid was washed with methanol and water to remove all physisorbed species (until the washings were colorless) and dried overnight at 80 °C. The SBA-15 support was prepared according to the procedure reported in a previous work [8].

(Insert Fig. 1 here)

2.4 HMF oxidation.

The catalytic activity performance of the metal Salen complexes supported on SBA-15 (Co/SBA-15, Fe/SBA-15 and Cu Salen/SBA-15) in the oxidation of HMF were evaluated. The HMF oxidation reaction was carried out in an aqueous system at neutral pH (the pH was not adjusted) using H₂O₂ as oxidant agent. The reaction was performed under mild conditions (aqueous media, neutral pH, atmospheric temperature and pressure). The system consisted of a 125 mL round-bottom flask with a refrigerant column to avoid the HMF volatilization. All tests were performed with an initial substrate HMF 0.4 mM [8], 50 mL reaction volume, H₂O₂ 30 w/V % (100 µL) as oxidant agent and using 0.05 g of catalyst. Aliquots of 500 µL were taken during 24 h, from which 75 µL were injected in the chromatograph for their analysis. The samples were taken in short periods of time at the early minutes of the reaction, and in a longer period as the reaction advanced in order to have enough information for the kinetic study. The reaction mixture was stirred at a constant 500 rpm. Tests were done at low temperatures 25, 30 and 40 °C to know how the temperature affects the reaction. Although the catalyst can be used at higher moderate temperatures, 40 °C level was selected as the maximum temperature to avoid H₂O₂ degradation. Temperature levels were recorded with thermocouples previously connected to a temperature monitoring program using the Labview System Design Software.

3. RESULTS AND DISCUSSION

3.1 Catalyst characterization

The different metallic Salen complexes Co (II), Cu (II) and Fe (III) were synthesized and immobilized by covalent bonds onto synthetic silica SBA-15. To follow synthesis and characterization of the catalysts, Fourier transform infrared spectroscopy (FTIR), UV-Visible spectroscopy (UV-Vis), Diffuse reflectance UV-Visible spectroscopy (DR-UV-Vis) and X ray photoelectron spectroscopy (XPS) were performed. UV-Visible absorption spectra confirmed the formation of the Salen ligand and its coordination with the corresponding metallic atom. FTIR spectra showed incorporation of metallic Salen complexes and its anchoring to the support was confirmed by DR-UV-Vis. Metallic content (from the complex) over the catalyst was obtained with atomic absorption spectroscopy (AAS); scanning electron microscopy (SEM) confirmed the synthesis of mesoporous hexagonal SBA-15, along with the textural properties results obtained from nitrogen physisorption characterization.

3.1.1 Fourier transform infrared spectroscopy (FT-IR)

Fig. 2 shows the spectra of Co Salen/SBA-15, Fe Salen/SBA-15 and Cu Salen/SBA-15 catalysts, along with the support without the complex (SBA-15), for comparative reasons. The catalyst spectra show a particular band at 1635 cm^{-1} attributed to $\nu(\text{C}=\text{N})$ stretching vibration, with a shift to lower frequency for the complexes, indicating coordination of azomethine nitrogen [48-50]. In this case, the band is showed at for Co Salen/SBA-15 and Cu Salen/SBA-15 but not for Fe Salen/SBA-15 probably due to its lower concentration. SBA-15 support showed intense and broad signals at 1000-1300, and 800 cm^{-1} , assigned to SiO_2 structure, which remains present after complex immobilization.

The signal at 950 cm^{-1} , associated with Si-OH bonds, decreases after complex immobilization, which implies that -OH groups have been consumed due to the anchoring of the complex over silica via chemical bond [51].

Once the complex has been anchored, the bands at 1300-1600 cm^{-1} can be associated with the existence of organic ligands. The band at 1544 cm^{-1} is attributed to azomethin group vibrations (H-C=N), which is a characteristic signal of Salen ligands [8]. IR spectra showed some evidence of complex anchoring, which was confirmed by DR-UV-Vis analysis.

(Insert Fig. 2 here)

The Fe complex catalyst spectra showed more differences, since the bands associated with the organic ligand can be difficult to observe. This may be explained due to a lower metallic loading for this catalyst (according to elemental analysis described below).

3.1.2 UV-visible spectroscopy (UV-vis)

Fig. 3 shows the formation of imine by comparing UV-Vis spectra obtained from the collected samples at different times over the synthesis, to subsequently give rise to the metal Salen complex formation according with the metal precursor used. Bands observed in the 200-400 nm range are attributed to $\pi-\pi^*$ and $n-\pi^*$ ligand charge transfer behavior [48, 52-54]. APTES, salicylaldehyde and salicylaldehyde-APTES mixture were dissolved in methanol and analyzed. No signals were observed for APTES (Fig. 3a). Salicylaldehyde (Fig. 3b) showed three bands at 212, 250 and 325 nm, similar to salicylaldehyde-APTES (Fig. 3c), but with a small shift to the red (2 nm) for the first and second signals. Additionally, a decrease in band intensity due to presence of APTES was observed. As soon as salicylaldehyde is in contact with APTES, a free imine is formed; a change in color from transparent to yellow evidenced this event. Three bands at 220, 254 and 315 nm were observed in the sample taken after stirring the salicylaldehyde-APTES and methanol mixture for 3 h, while a new band at 405 nm appears due to the formation of the free imine.

(Insert Fig. 3 here)

In Fig. 4, the UV-Vis spectra of different metallic Salen complexes Fe(III), Cu(II) and Co(II) (unsupported) are compared. The dotted lines represent the spectrum after 3 h stirring once the metal precursor was added and continuous lines signify the spectra after an additional 15 h stirring. In the Co Salen complex spectrum (Fig. 4c) three bands at 230, 265 and 365 nm were observed. The Cu Salen complex spectrum (Fig. 4b) showed four bands at 230, 273, 305 and 363 nm, while for the Fe Salen complex spectrum (Fig. 4a) bands at 243, 263, 330 and 410 nm are observed. All complexes showed bands between 230 and 273 nm, which are attributed to π - π^* charge transfers. The signals between 305 and 365 nm are assigned to n - π^* charge and the small band from Fe Salen at 410 nm can be attributed to ligand to metal charge transfers. The band around 363-365 nm was assigned to charge transfer transition from the Salen ligand [55]. This indicates the formation of the Salen ligand and the decrease of the free imine band once the Salen ligand signal appears, confirming imine coordination forming the Salen metallic complex [56]. A characteristic absorption band at approximately 450 and 550 nm, attributed to d-d charge transfer transitions from the Co atom, was not observed due to the low concentration of the Salen metallic complex, since the synthesis was carried out in an excess of methanol [55]. For this work, all catalysts were prepared using the same methodology. The reacting solution was stirred for 15 h, and finally the solvent was separated using a rotary evaporator. Since spectra after 3 h and an additional 15 h stirring are very similar, it is possible that the stirring time can be reduced in order to evaluate the difference in catalytic activity.

(Insert Fig. 4 here)

3.1.3 Diffuse reflectance UV-visible spectroscopy (DR-UV-Vis)

DR-UV-Vis spectra for the different metal Salen complex catalysts are observed in Fig. 5. The spectrum for pure SBA-15 support (Fig. 5d) is also shown for comparison. Characteristic signals can be observed at 280 nm for Co Salen/SBA-15 (Fig. 5c), and 270 nm for Cu Salen/SBA-15

(Fig.5b) and Fe Salen/SBA-15 (Fig. 5a); both bands are attributed to π - π^* from the phenyl ring of the Salen ligand. Signals at 370 nm for Cu and at 390 nm for Co and Fe, were related with n - π^* transitions from azomethine (C=N). A shoulder was observed at 460 nm for Co and Cu due to charge transference between metal and nitrogen; additionally, bands at 620 and 650 nm for Co and Cu respectively were related with d-d transitions. For the Fe Salen/SBA-15 catalyst, a shoulder was observed at 500 nm, and the signal at 600 nm was not observed, possibly due to an overlapping or a smaller complex content over SBA-15, which was found in elemental analysis. The mentioned signals are a clear indicative of the metallic complexes being supported over SBA-15, according with the previously reported for metal Salen complexes supported [7, 57-59]. The different λ values found for different catalyst may be explained due to their varying nature and structure; Co (II) and Cu (II) Salen complexes usually present a flat square structure, while Fe (III) Salen complex is associated to a square pyramidal structure [60-62].

(Insert Fig. 5 here)

3.1.4 Elemental analysis by Atomic absorption spectroscopy (AAS)

All different solid catalysts Co, Cu and Fe Salen complexes supported over SBA-15 were submitted to acid digestion and AAS evaluation. The metallic loading (mmol metal/g catalyst) over the support was Cu (0.22 mmol/g) > Co (0.20 mmol/g) > Fe (0.18 mmol/g). This may be related with atomic radiuses of the metals: Fe (1.72 Å) > Co (1.67 Å) > Cu (1.57 Å), and atomic weight of Cu (63.55 g/mol) > Co (58.93 g/mol) > Fe (55.85 g/mol). The Cu Salen complex seems to have a smaller size (being the element with the lowest atomic radius), which could promote dispersion and further facilitate anchoring over the hexagonal channels of SBA-15 in comparison with the Fe Salen complex, being the Fe which has the largest atomic radius of the three metals. Therefore a better catalytic performance with Cu Salen catalyst is expected.

3.1.5 N₂ adsorption/desorption isotherms and textural analysis.

Fig. 6 shows adsorption and desorption isotherms for the SBA-15 support and Fe Salen/SBA-15, Cu Salen/SBA-15 and Co Salen/SBA-15 catalysts at 77 K. All the plots showed are isotherms Type IV, which are characteristic of mesoporous materials. A clear step was observed for pore filling, which indicates the presence of a narrow pore size distribution [63, 64]. The hysteresis cycle showed a behavior similar to H1 and H2 types; more specifically, H1 type for SBA-15 and H2 type for the rest of the catalysts. However, for the Fe Salen/SBA-15 catalysts hysteresis was more similar to that of the pure SBA-15 (H1), which may be related with a lower complex charge over the support (which was confirmed with elemental analysis). H1 type hysteresis is frequently associated with porous materials consisting on agglomerates with nearly uniform arrangements, which tend to show a narrow pore size distribution, while H2 type is more associated with unordered pores, where pore size distribution and shape are not very well defined [65]. It can be caused due to the complex incorporation; however, for this case all samples showed a narrow distribution. It can also be observed that the hysteresis loops of all samples begin at $p/p_0 = 0.4$ and end at $p/p_0 = 0.7$, suggesting limited adsorption. This phenomenon is related to the presence of particles that are not rigidly joined together [66]. The SBA-15 (Fig. 6) reached the highest value of adsorption at the saturation point ($p/p_0 = 1$) followed by Fe Salen/SBA-15, Co Salen/SBA-15 and Cu Salen/SBA-15; which is related to the greater surface area, as shown in Table 1, and the better interconnection of pores within the particles, which can favor percolation phenomena [66]. Nevertheless, the metal Salen complex is responsible for the activity and the aforementioned confirm the anchoring of the metal Salen complexes in the SBA-15 channels.

(Insert Fig. 6 here)

In Fig. 7, pore distribution for support and different catalysts are shown. A small shift can be observed at the right side of the peak, which is more prominent for Cu and Co catalysts. This may

be related with complex incorporation over the support; the Salen complex enters inside the biggest pores, decreasing the available spaces. This may also be related with a higher peak maximum. It is widely known that SBA-15 hexagonal mesoporous silica is interconnected with nonuniform micropores [63]; this was observed at low relative pressures (p/p_0). A wider space can be observed between adsorption and desorption isotherms at low p/p_0 for catalysts, compared with the pure support. This may be due to micropore formation during the catalyst drying process, which promotes water and methanol evaporation from the catalyst surface. The isotherms of all samples observed on Fig.6 confirm the SBA-15 support channels remain accessible [57].

(Insert Fig. 7 here)

Table 1 summarizes the textural properties of the catalysts and SBA-15 support. It is widely known that a high specific surface area is desired for heterogeneous catalysis applications in order to promote active phase dispersion; having a higher surface area will also promote adsorption and desorption processes. However, a bigger surface area does not guarantee a better catalytic behavior. Textural properties obtained for SBA-15 material were: a specific surface area $S_{\text{BET}} = 583 \text{ m}^2/\text{g}$, average pore diameter $D_p = 3.81 \text{ nm}$ and pore volume $V_p = 0.67 \text{ cm}^3/\text{g}$. All of these data agree with previous reports by other authors [57, 64, 67, 68]. After the metallic Salen complex was immobilized over the SBA-15 support, no significant changes were observed in average pore sizes, while specific surface area and pore volume showed a prominent decrease, in the order SBA-15 > Fe Salen/SBA-15 > Co Salen/SBA-15 > Cu Salen/SBA-15. This may suggest that metal Salen complex was mainly grafted inside the mesoporous support surface [53, 55]. The wall thickness may have been increased when the catalyst was anchored over the support, since the complex is mainly located over the inner surface of mesoporous materials [48]. When the complex is supported, the pore diameter distribution is narrower than that of pure SBA-15, suggesting that the anchorage of the complex occurs in the larger pores. The decrease in pore volume and specific surface area after complex immobilization indicates the complex was grafted inside the mesoporous silica channels [55, 69].

3.1.6 SEM

In Fig. 8 (with scale of 200 nm) hexagonal channels are observed, with an average pore size of 4.4 nm, compared with 3.81 nm calculated from the N₂ physisorption analysis. This morphology is characteristic of SBA-15 materials due their synthesis with the template (surfactant Pluronic P123).

(Insert Fig. 8 here)

3.1.7 X-ray photoelectron spectroscopy (XPS)

To get deeper insight into the surface constitution of the catalysts and the oxidation states of the elements, the C1s, N1s, O1s and M 2p (M= Cu, Co or Fe) binding energies were investigated. For this purpose, Fig. 9 and Fig. 10 show the high energy resolution XPS spectra of the elements mentioned. The C 1s spectrum can be deconvoluted in three peaks, for Co Salen/SBA-15 (Fig. 9a) the peak at 284.7 eV is attributed to both aromatic and aliphatic carbons of the salen ligand [70]; a peak at 286.5 eV is associated with C – O or C – N and the low intensity band at ca. 289 eV can be related to a shake-up satellite associated with $\pi - \pi^*$ transitions in the aromatic carbon rings of the ligand [70]. The C1s spectrum for Cu Salen/SBA-15 (Fig. 9b) also showed three peaks at similar positions 284.7, 286.3 and 288.7 eV and as well as 284.5, 286.7 and 289 eV for Fe Salen/SBA-15 (Fig. 9c) respectively. These results suggest that although Salen complexes can represent the same kind of interactions with different metallic species, the aromatic rings can modify the electron density in the conjugated π -system in the three different systems leading to a potential charge increase and causing a shift to the negative region [71].

N1s spectrum can be deconvoluted also into three peaks, the first one is attributed to the binding energy between metal and nitrogen (M – N) [72] at 399.5, 399.2 and 399.7 eV for Co Salen/SBA-15 (Fig. 9a), Cu Salen/SBA-15 (Fig. 9b) and Fe Salen/SBA-15 (Fig. 9c) respectively. Second peak at 400.8 (Fig. 9a), 400 (Fig. 9b) and 401.7 eV (Fig. 9c) is associated with C = N [73] and the last one

and the last one at 402.8 (Fig. 9a), 403 (Fig. 9b) and 403.5 (Fig. 9c) is attributed to the Salen ligand nitrogen [73].

The XPS spectra in the O1s region show an intense peak around 532 eV which can be deconvoluted in three peaks. The first is associated to the energy binding between metal and oxygen (M – O) [70] at 530.5, 531.7 and 532.5 eV as is showed in the O1s spectrums in Fig. 9a, b ,c for Co Salen/SBA-15, Cu Salen/SBA-15 and Fe Salen/SBA-15 respectively. The second at 532.5 eV for Co Salen/SBA-15 and Cu Salen/SBA-15 catalysts (Fig. 9a, b) and 532.7 eV for Fe Salen/SBA-15 (Fig. 9c) can be attributed to C–O binding energy from the metal-Salen complex [74] and also for Si – O binding energy [75] from the SBA-15 matrix; this is why it is the most intense peak, since the binding energy between the Si – O bond of silica predominates. The third peak at 533.3, 533.5 and 534 eV (Fig. 9 a,b,c) is due to the O – H in the surface [75]. The binding energy exhibited in the spectra confirms the formation of the metal Salen type catalysts

The elemental analysis results from the atomic absorption spectroscopy showed a loading (mmol/g) Cu > Co > Fe which can be related to the anchored metal Salen complex, due to this analysis is from the bulk and the XPS is a surface analysis, the variation in the intensity of the C1s and N1s spectra being higher for Cu Salen/SBA-15 catalyst followed by Co Salen/SBA-15 and Fe Salen may be due to the anchorage of Cu Salen is favored more within the pores of the SBA-15 than on the surface.

Figure 10 shows the M2p high resolution XPS spectrum for each catalyst where two peaks associated to 2p 3/2 and 2p1/2 spin-orbit levels can be seen. Co 2p spectrum (Fig. 10a) shows two peaks from the Co 2p3/2 at 781.5 and Co 2p1/2 at 797 eV attributed to Co – N from Co (II) Salen complex supported and satellite bands at 787 and 802.3 eV [48, 76-78]. Cu 2p spectrum (Fig. 10b) exhibits two peaks at 932.7 and 952.5 eV attributed to Cu 2p3/2 and Cu 2p1/2 from Cu (II) Salen complex supported and low intensity bands around 940 and 945 eV associated to satellites [48, 60]. Fe 2p spectrum (Fig. 10c) shows two deconvoluted peaks attributed to Fe 2p3/2 and Fe 2p1/2 with a maximum around 711 and 723.5 eV respectively, which shows peaks at 711 and 723.5 eV associated to Fe (II) while the peaks at 714.3 and 726 eV can be related to Fe (III) species [48, 75,

79]; with satellites at 718.7 and 730.5 eV. Satellite lines and the separation of the 2p_{3/2} and 2p_{1/2} spin-orbit levels often provide valuable information concerning the oxidation state and electronic structure of metal ions [48]. For the studied catalysts the separation between the peaks that correspond to 2p_{3/2} and 2p_{1/2} spin-orbit levels were 15.5, 19.8 and 12.5 eV for Co, Cu and Fe (metal Salen/SBA-15 catalysts) respectively nearly to the reported (from Co (II), Cu (II) and Fe (III) tetrahydro Salen and Salen complex onto amino-functionalized SBA-15) by other authors [48, 80]. In the other hand, the presence of satellite lines in 2p_{3/2} and 2p_{1/2} spin-orbits is indicative of a high-spin of the metallic center [48].

For metal oxides, the expected binding energies are around 933.2-933.1 eV (in presence of shake up satellites) for Cu 2p_{3/2} from CuO, a peak between 933-933.8 eV (in absence of shake up satellites) for Cu 2p_{3/2} from Cu₂O and a peak at 954 eV is related to Cu 2p_{1/2} [81, 82], while the Cu Salen/SBA-15 catalyst studied showed peaks at a lower energy (932.7 and 952.5 eV) . For CoO and Co₃O₄ species binding energies have been reported between 779.6-780.6 eV and 794.5-796.4 eV associated to Co 2p_{1/2} and 2p_{3/2} respectively, while a peak at 778.1 eV is due to metallic cobalt [83, 84]. In contrast to Co 2p peaks and t higher energy (781.5 and 797 eV) from Co Salen/SBA-15 catalyst. From the Fe 2p results it may be apparent that different species of iron complex are present.

Finally, a relationship between XPS and other characterization techniques with the activity potential for each catalyst will be made. The third peak from O1s spectra (attributed to O – H in the surface) shows a larger area for Cu Salen/SBA-15 catalyst (Figure 9b), compared with Co (Figure 9a) and Fe (Figure 9c) Salen supported catalysts, whose areas for the same peak are 21 and 29% shorter than the area for Cu Salen catalyst, respectively. This indicates that more O-H groups are available on the surface of the Cu Salen/SBA-15 catalyst, which agrees with the observed in N1s spectra, where the first peak (associated to M – N) presents a higher intensity for Co Salen/SBA-15 catalyst, which is related to a larger amount of metal Salen complex in the surface. The Fe Salen/SBA-15 catalyst shows a lower amount of complex in the surface (related with a smaller N1s peak intensity), while the Cu Salen shows the lowest amount of complex from all the catalysts. As stated before,

from the AAS and N₂ physisorption analyses, the Cu Salen catalyst showed the highest metal loading and the lowest specific surface area. This suggests that the Cu Salen complex is anchored inside the hexagonal channels of the SBA-15 support, and a better dispersion was apparently achieved with this catalyst, which contributes to a better catalytic performance.

(Insert Fig. 9 here)

(Insert Fig. 10 here)

3.2 Catalytic activity of metal (Co II, Fe III and Cu II) Salen complex in HMF oxidation under mild conditions.

.3.2.1 Effect of the transition metal of the metal Salen complex on HMF oxidation

In order to evaluate the effect of the transition metal present in the catalyst, the catalysts Co Salen, Cu Salen and Fe Salen supported on SBA-15 were tested. The activity tests with an initial substrate concentration of 0.4 mM, 0.050 g of catalyst and 100 μ L of H₂O₂ 30 w/V %; at 30 °C were performed. In the Fig. 11 a significant difference with the Co Salen/SBA-15 catalyst can be observed, which showed a lower performance with an HMF conversion around 40%, while with the others (Fe Salen/SBA-15 and Cu Salen/SBA-15), a conversion around 100 % was reached. For Cu Salen/SBA-15 the reaction rate was slightly higher in the early minutes. An explication of the higher activity, $\text{Cu}^{2+} > \text{Fe}^{3+} > \text{Co}^{2+}$ could be related with the standard electrode potential values (E_0), being more positive for Cu^{2+} with $E_{0 \text{ Cu}^{2+}/\text{Cu}} = + 0.34 \text{ V}$ and more negative for Co^{2+} with $E_{0 \text{ Co}^{2+}/\text{Co}} = - 0.29 \text{ V}$, while for Fe^{3+} $E_{0 \text{ Fe}^{3+}/\text{Fe}} = - 0.04$; this means that Cu^{2+} is more oxidant than Fe^{3+} and Co^{2+} . On the other hand, a higher activity was expected with Cu Salen/SBA-15 catalyst, due to a higher metal loading and a better dispersion achieved with this metal Salen complex over the support, which favor its catalytic activity, as previously mentioned in section 3.17. However, differences in the molecular structure of the different complexes and their nature (depending on the used precursor)

could also contribute to the catalyst to have a better or poor performance in catalytic activity. It is worth mentioning that after a physical observation, the Fe Salen/ SBA-15 catalyst was the least stable, since during the reaction course its yellowish color was lost and it became almost completely white, similar to the pure support. With the foregoing the Cu Salen/SBA-15 was selected to continue with the activity test applied in the HMF oxidation. It is considered as a good finding for this reaction, where metals such as Fe and Cu showed an increased catalytic performance compared with Co (known for its high activity in catalysis and one of the most studied Salen complexes, although in homogeneous catalytic reactions), known as toxic and harmful to health and environmental for a high concentration of exposition.

(Insert Fig. 11 here)

3.2.2 Effect of the H₂O₂ amount on HMF oxidation with Cu Salen/SBA-15

Fig. 12 shows comparative plots to study the effect of the amount of H₂O₂, using the catalyst Cu Salen/SBA-15. It was observed that the amount of H₂O₂ had a significant effect on the conversion rate, reaching 100% of HMF conversion using 100 μ L of H₂O₂ 30% w/V compared to about 5% with 5 μ L of H₂O₂ 30% w/V. Based on the foregoing, the experimental activity tests were performed using 100 μ L H₂O₂. It can also be observed that the reaction goes from 0 to 74% of conversion in the first 50 minutes, later becomes slower.

(Insert Fig. 12 here)

3.2.3 Effect of the temperature on HMF oxidation with Cu Salen/SBA-15

Activity tests at different temperatures were performed in order to know its effect in the HMF oxidation with Cu Salen/SBA-15. These experiments were performed with an initial HMF concentration of 0.4 mM, 100 μ L of H₂O₂ 30 w/V % and 0.050 g of Cu Salen/SBA-15 catalyst, during 24 h approximately. The temperatures evaluated were 25, 30 and 40 °C as maximum in

order to avoid the H₂O₂ degradation. As can be observed in the Fig. 12, a significant difference is not observed in this range of temperatures with the rate reaction and HMF percent conversion for all cases the conversion reached nearly 100%. This reveals that the reaction can be carried out at room temperature and that if temperature changes during the reaction, it will not significantly change the catalytic performance, at least in the studied range.

(Insert Fig. 13 here)

3.2.4 Kinetic study of HMF oxidation with Cu Salen/SBA-15

In Fig. 14 a change in the concentration was observed during the course of the reaction (around 24 h) for HMF and the identified products DFF, FDCA, HMFC and FFCA. For the mentioned experimental tests, the Cu Salen/SBA-15 catalyst was evaluated. A rapid disappearance of HMF during the first 200 min is observed, to stabilize close to 0 mM. For the products, the maximum was reached between 50-100 min. After this the concentration dropped; an explanation could be that the reaction continued to form more oxidized products (unidentified). From the identified products by the developed analytical method (HPLC), it was observed that before the concentration dropped under the condition of study ($C_{\text{HMF } 0} = 0.4 \text{ mM}$, 100 μL of H₂O₂ 30 w/V %, 0.050 g of Cu Salen/SBA-15 at 30 °C), the selectivity was higher for FDCA and DFF products; while it was lower for HMFC and FFCA and very similar between this both last products.

(Insert Fig. 14 here)

Consequently, it was noted that the reaction under the established conditions was selective to other products, different to the identified by the HPLC separation method previously developed. However, the kinetic analysis was continued with the information obtained during the first 100 min of the reaction, to study the kinetics before the decrease in products concentration; since there is no monitoring of the unidentified products.

To observe the behavior of the obtained curves where the product concentrations increase, reaching a maximum at the same time and not a curve that grows and decays while another appears according to the literature [85], a mechanism with parallel reactions was proposed as follows (Fig. 15).

(Insert Fig. 15 here)

The respective rate reaction equations for each compound were proposed as follows.

For HMF, the rate reaction ($-r_{HMF}$) is expressed:

$$r_{HMF} = - \frac{dC_{HMF}}{dt}$$

Equation 1

$$\frac{-dC_{HMF}}{dt} = k_1 C_{HMF} + k_2 C_{HMF} + k_3 C_{HMF} + k_4 C_{HMF}$$

Equation 2

Where the negative sign indicates that HMF is disappearing, $\frac{-dC_{HMF}}{dt}$ is the HMF concentration change with time, C_{HMF} is the HMF concentration at an arbitrary time. The kinetic constants k_1 , k_2 , k_3 y k_4 correspond to the HMF reaction to produce DFF, FDCA, HMFCa and FFCA respectively.

By grouping the kinetic constants $k = k_1 + k_2 + k_3 + k_4$, then remain

$$\frac{-dC_{HMF}}{dt} = k C_{HMF}, \text{ integrating and replacing the initial conditions } t = 0$$

and $C_{HMF} = 0.4 \text{ mM}$ it was obtained the equation for C_{HMF} .

$$C_{HMF} = 0.4 e^{-kt}$$

Equation 3

For DFF, FDCA, HMFCa and FFCA products, differential rate reaction equations remain as follows:

$$r_{DFE} = \frac{dC_{DFE}}{dt} = k_1 C_{HMF}$$

Equation 4

$$r_{FDCA} = \frac{dC_{FDCA}}{dt} = k_2 C_{HMF}$$

Equation 5

$$r_{HMFA} = \frac{dC_{HMFA}}{dt} = k_3 C_{HMF}$$

Equation 6

$$r_{FFCA} = \frac{dC_{FFCA}}{dt} = k_4 C_{HMF}$$

Equation 7

Where it can be seen that the sign is positive, since these are products formed. Integrating the above equations and substituting for $t = 0$ when only HMF is present and the initial concentrations of the products C_{DFE} , C_{FDCA} , C_{HMFA} and C_{FFCA} are zero:

$$C_{DFE} = \frac{0.4k_1}{k} (1 - e^{-kt})$$

Equation 8

$$C_{FDCA} = \frac{0.4k_2}{k} (1 - e^{-kt})$$

Equation 9

$$C_{HMFC A} = \frac{0.4k_3}{k} (1 - e^{-kt})$$

Equation 10

$$C_{FFCA} = \frac{0.4k_4}{k} (1 - e^{-kt})$$

Equation 11

After calculating the integrated equations for each concentration, these were used to make the fitting using Matlab software (version R2016a) using the Curve Fitting tool. Fig. 16, shows the concentration curves versus time for HMF and the identified products from the catalytic oxidation in presence of H₂O₂ and the Cu Salen/SBA-15 catalyst with C_{HMF 0} = 0.4 mM at 30°C. The points represent the experimental data and the lines the first fitting with the proposed kinetic model (Equations 3 and 8-11).

-

(Insert Fig. 16 here)

Fig. 16, shows that a good fitting for the products experimental data was obtained. For HMF, although has the same behavior that the experimental data, this does not pass through all the data as in the case of products (DFF, FDCA, HMFC A and FFCA).

The Table 2 bellow present the kinetic constants k_1, k_2, k_3, k_4 y k ; obtained from the model fit.

It is notable that the kinetic constant $k \neq k_1 + k_2 + k_3 + k_4$, this because they are giving additional reactions in parallel, then $k = k_1 + k_2 + k_3 + k_4 + k_x$. Where k_x would be a kinetic constant from contributions from additional constants due to the reactions that occur for the formation of products that are not able to identify at the moment and according to the literature could be happening something similar to what is shown in Fig. 17 [28]. The reason why the

experimental data suggests that the products are being formed through parallel reactions from the oxidation of HMF of the alcohol and aldehyde group of the HMF molecule might be due to the oxidation steps from DFF and FFCA oxidation are occurring faster and then is possible to observe the FDCA and FFCA products from the first minutes of the reaction.

(Insert Fig. 17 here)

This is an explanation of why a better fit of the experimental data (C_{HMF} against time) was not fully achieved, because additional information about other reactions occurring (which were not used in the deduction of the proposed mechanism) would be needed.

Table 3 shows a summary of HMF % conversion and % selectivity to the identified products DFF, FFCA, FDCA and HMFCA for the different activity conducted tests.

There is a synergistic effect between the Salen/SBA-15 and Fe Salen/SBA-15 catalysts with the H_2O_2 , due to the conversion percentage achieves almost 100% compared with 40% in catalyst absence, but it is important to denote that the Fe Salen/SBA-15 was dissolved and acted in homogenous reaction. The selectivity of the identified products DFF and FDCA were higher than the others in all the cases using 100 μL of H_2O_2 . However, for Cu and Fe, FDCA conversion was the highest. This can be explained due to FDCA having two carboxylic acid groups; this molecule is the maximum oxidation state of HMF. It is also at the end of the sequential reactions, which means the environment was oxidant enough to promote a high conversion of DFF and FFCA to FDCA.

The molecule with the least conversion was HMFCA, which is expected due to the difficult of having oxidizing conditions that can both oxidate the aldehyde group of HMF completely to carboxylic acid, but leave the alcohol group intact. This would suggest that the studied reaction system was favored by oxidation of the alcohol side of the HMF molecule to form DFF (aldehyde) followed by FFCA that is converted rapidly to FDCA (Fig. 18). Oxidation of the aldehyde side of the HMF molecule to form HMFCA is not as promoted as previously explained, and therefore only few FFCA and FDCA could have been obtained through this mechanism (Fig. 19).

(Insert Fig. 18 here)

(Insert Fig. 19 here)

3.3 Stability test of Cu Salen/SBA-15 catalyst

Before using the catalyst in the reaction, it was stirred for 15 h in deionized water, it was then recovered and dried at 80 °C for 15 h, and this was called mechanical treatment. All further tests (already discussed in this manuscript) were performed with the catalysts after mechanical treatment. For stability tests, spectroscopic analysis of atomic absorption and DR-UV-vis were performed for the catalyst before and after reaction (this catalyst was recovered and dried following the same process described above). Recycle tests were performed using an HMF concentration of 0.4 mM, a 30% H₂O₂ volume of 100 µL and 0.05 g of the Cu (II) Salen/SBA-15 catalyst, with atmospheric pressure. Each cycle lasted for 24 h.

3.3.1 Atomic absorption spectroscopy (AAS)

From the AAS, a copper loading of 0.14 mmol Cu/ g catalyst and 0.024 mmol Cu/g catalyst were obtained for the catalysts before and after reaction, respectively. This indicates that leaching of the active species is happening, which was confirmed by the presence of copper in the reaction solution. Consequently, it could be asked, what is acting as a catalyst? Are the active species in the solid, liquid or in both phases? For every experiment, once the samples were centrifugated and the separated liquid was taken for HPLC evaluation, repeated measurements at different times up to about 24 hours, showed no changes in concentration. Therefore, we can conclude that despite leaching, the solid catalyst (supported metal Salen complex) was identified as the active species in the reaction and not the species in solution, discarding the latter as catalytically active.

3.3.2 Recycle tests

Fig. 20 shows the results from the recycle tests performed for the reaction. A slight decrease in the HMF conversion is present, with a difference of only 2.7% between the first and final cycle.

(insert Figure 20 here)

3.3.3 DR-UV-vis spectroscopy

Fig. 21 illustrates the DR-UV-vis spectrum of the Cu Salen/SBA-15 catalyst before and after being used in the reaction and also the corresponding spectrum to the pure support SBA-15 for comparative purposes. Fig. 21b shows the characteristic Cu Salen/SBA-15 catalyst bands, already discussed before. Fig. 21c shows the Cu Salen/SBA-15 catalyst after reaction, where the same catalyst bands are observed, but with a marked intensity decrease.. Therefore, and although these catalysts showed good activity and recyclability, it is still necessary to continue the study of such catalysts to improve their stability.

(insert Figure 21 here)

CONCLUSIONS

Salen catalyst complexes of Fe (III) and Cu (II) supported on SBA-15 were the most active in the oxidation of HMF using H_2O_2 as an oxidizing agent; however, the Fe (III) presented low stability, so more studies are needed to have a better understanding of its catalytic performance. Cu Salen/SBA-15 catalyst, although present leaching, showed the best activity due to the highest metal loading (Cu Salen complex) and mainly because of a better dispersion of the active phase. H_2O_2 played an important role in the reaction, since it significantly affects the conversion and selectivity. However, it has a synergistic effect with the catalyst which was found when the conversion did not exceed 40% when only carried out with H_2O_2 alone, while when both the catalyst and the peroxide were present, a conversion close to 100% was reached. Under the reaction conditions, the HMF oxidation was more selective towards unidentified products; it is presumed that this occur due to the furan ring rupture. With the decrease in the amount of H_2O_2 and therefore HMF conversion, the selectivity to DFF, FDCA, FFCA and HMFCA products increased. A good fit to the identified products (DFF, FDCA, HMFCA and FFCA) with the proposed mechanism with parallel reactions was achieved, however, for the HMF the adjustment was not perfect due to the lack of information

about other formed products. However, differences in the molecular structure and transfer energy could also affect their performance, which may be related to that observed in the DR-UV-Vis spectra, where the different bands of electronic transitions $\pi\text{-}\pi^*$, $n\text{-}\pi^*$ and metal-N (center of the ligand) are well-defined for the copper complex, while for the other catalysts are given overlaps. The behavior of the curves from the experimental data of the identified products (DFF, FDCA, HMFA and FFCA) indicates that their formation is being carried out by parallel reactions or the DFF and FFCA oxidation are very fast reaction steps. On the other hand, a good fit to the experimental data on the concentration of HMF was not achieved, since more information of the other occurring reactions is required. It is suggested that the products were not identified until now are a result of the rupture of the furan ring. Metal Salen complex Co, Cu and Fe catalysts showed a higher selectivity towards the formation of DFF compared to HMFA, suggesting that is more favorable the oxidation of alcohol group in HMF molecule that oxidation of the aldehyde group in the other side of the molecule under the conditions here described. Metal Salen complex supported should remain a case study in catalysis since they have the advantage of being active at atmospheric pressure with green oxidizing agents and at room temperature.

ACKNOWLEDGEMENTS

This work was funded by Facultad de Ciencias Químicas, UANL. Daniela Xulú Martínez Vargas is very grateful to the National Council of Science and Technology (CONACYT) of Mexico for its support and for the scholarship awarded to the Postgraduate of Science Focused in Sustainable Processes at Universidad Autónoma de Nuevo León registered in the National Quality Graduate Program from the CONACYT key 000597. Daniela Xulú Martínez Vargas and Ladislao Sandoval Rangel now work at Tecnológico de Monterrey, Monterrey Campus, Research group in Energy and Climate Change. The authors thank to Dr. Carlos D. Garcia and to University of Texas at San Antonio (UTSA) for the facilities provided.

REFERENCES

[1] S. Albonetti, A. Lolli, V. Morandi, A. Migliori, C. Lucarelli, F. Cavani, Conversion of 5-hydroxymethylfurfural to 2,5-furandicarboxylic acid over Au-based catalysts:

- Optimization of active phase and metal–support interaction, *Applied Catalysis B: Environmental*, 163 (2015) 520-530.
- [2] F. Neațu, R.S. Marin, M. Florea, N. Petrea, O.D. Pavel, V.I. Pârvulescu, Selective oxidation of 5-hydroxymethyl furfural over non-precious metal heterogeneous catalysts, *Applied Catalysis B: Environmental*, 180 (2016) 751-757.
- [3] Y. Román-Leshkov, J.N. Chheda, J.A. Dumesic, Phase Modifiers Promote Efficient Production of Hydroxymethylfurfural from Fructose, *Science*, 312 (2006) 1933-1937.
- [4] L. Hu, G. Zhao, W. Hao, X. Tang, Y. Sun, L. Lin, S. Liu, Catalytic conversion of biomass-derived carbohydrates into fuels and chemicals via furanic aldehydes, *RSC Advances*, 2 (2012) 11184-11206.
- [5] D.M. Alonso, J.Q. Bond, J.A. Dumesic, Catalytic conversion of biomass to biofuels, *Green Chemistry*, 12 (2010) 1493-1513.
- [6] M. Vohra, J. Manwar, R. Manmode, S. Padgilwar, S. Patil, Bioethanol production: Feedstock and current technologies, *Journal of Environmental Chemical Engineering*, 2 (2014) 573-584.
- [7] N.-T. Le, P. Lakshmanan, K. Cho, Y. Han, H. Kim, Selective oxidation of 5-hydroxymethyl-2-furfural into 2,5-diformylfuran over VO₂⁺ and Cu²⁺ ions immobilized on sulfonated carbon catalysts, *Applied Catalysis A: General*, 464–465 (2013) 305-312.
- [8] D.X. Martíneza Vargas, J. Rivera De La Rosa, S. Arif Iyoob, C.J. Lucio-Ortiz, F.J. Cerino Córdoba, C.D. Garcia, Phenol oxidation by air using a Co (II) Salen complex catalyst supported on nanoporous materials: synthesis, characterization and kinetic analysis, *Applied Catalysis A: General*, 506 (2015) 44-56.
- [9] G.W. Huber, S. Iborra, A. Corma, Synthesis of Transportation Fuels from Biomass: Chemistry, Catalysts, and Engineering, *Chemical Reviews*, 106 (2006) 4044-4098.
- [10] A. Corma, S. Iborra, A. Velty, Chemical Routes for the Transformation of Biomass into Chemicals, *Chemical Reviews*, 107 (2007) 2411-2502.
- [11] L. Bing, Z. Zhang, K. Deng, Efficient One-Pot Synthesis of 5-(Ethoxymethyl)furfural from Fructose Catalyzed by a Novel Solid Catalyst, *Industrial & Engineering Chemistry Research*, 51 (2012) 15331-15336.
- [12] S.P. Simeonov , J.A.S. Coelho , C.A.M. Afonso An Integrated Approach for the Production and Isolation of 5-Hydroxymethylfurfural from Carbohydrates, *ChemSusChem*, 5 (2012) 1388-1391.
- [13] A.D. Sutton, F.D. Waldie, R. Wu, M. Schlaf, L.A. ‘Pete’ Silks, J.C. Gordon, The hydrodeoxygenation of bioderived furans into alkanes, *Nat Chem*, 5 (2013) 428-432.
- [14] R.-J. van Putten, J.C. van der Waal, E. de Jong, C.B. Rasrendra, H.J. Heeres, J.G. de Vries, Hydroxymethylfurfural, A Versatile Platform Chemical Made from Renewable Resources, *Chemical Reviews*, 113 (2013) 1499-1597.
- [15] B. Liu, Z. Zhang, K. Lv, K. Deng, H. Duan, Efficient aerobic oxidation of biomass-derived 5-hydroxymethylfurfural to 2,5-diformylfuran catalyzed by magnetic nanoparticle supported manganese oxide, *Applied Catalysis A: General*, 472 (2014) 64-71.
- [16] T. Werpy, G. Peterson, Top Value Added Chemicals from Biomass, U.S. Department of Energy (DOE), Springfield, VA, (2004) 22161.
- [17] B. Kamm, Production of Platform Chemicals and Synthesis Gas from Biomass, *Angewandte Chemie International Edition*, 46 (2007) 5056-5058.
- [18] K.T. Hopkins, W.D. Wilson, B.C. Bender, D.R. McCurdy, J.E. Hall, R.R. Tidwell, A. Kumar, M. Bajic, D.W. Boykin, Extended Aromatic Furan Amidino Derivatives as Anti-Pneumocystis carinii Agents, *Journal of Medicinal Chemistry*, 41 (1998) 3872-3878.

- [19] M. Del Poeta, W.A. Schell, C.C. Dykstra, S. Jones, R.R. Tidwell, A. Czarny, M. Bajic, M. Bajic, A. Kumar, D. Boykin, J.R. Perfect, Structure-In Vitro Activity Relationships of Pentamidine Analogues and Dication-Substituted Bis-Benzimidazoles as New Antifungal Agents, *Antimicrobial Agents and Chemotherapy*, 42 (1998) 2495-2502.
- [20] A.S. Benahmed-Gasmi, P. Frere, M. Jubault, A. Gorgues, J. Cousseau, B. Garrigues, Proceedings of the International Conference on Science and Technology of Synthetic Metals (ICSM'92) 2,5-bis(1,4-dithiafulven-6-yl) substituted furans, thiophenes and N-methyl pyrroles as precursors for organic metals, *Synthetic Metals*, 56 (1993) 1751-1755.
- [21] D.T. Richter, T.D. Lash, Oxidation with dilute aqueous ferric chloride solutions greatly improves yields in the '4+1' synthesis of sapphyrins, *Tetrahedron Letters*, 40 (1999) 6735-6738.
- [22] X. Tong, Y. Ma, Y. Li, Biomass into chemicals: Conversion of sugars to furan derivatives by catalytic processes, *Applied Catalysis A: General*, 385 (2010) 1-13.
- [23] J. Ma, Z. Du, J. Xu, Q. Chu, Y. Pang, Efficient Aerobic Oxidation of 5-Hydroxymethylfurfural to 2,5-Diformylfuran, and Synthesis of a Fluorescent Material, *ChemSusChem*, 4 (2011) 51-54.
- [24] C. Moreau, M.N. Belgacem, A. Gandini, Recent Catalytic Advances in the Chemistry of Substituted Furans from Carbohydrates and in the Ensuing Polymers, *Topics in Catalysis*, 27 (2004) 11-30.
- [25] C. Méalares, A. Gandini, Polymeric schiff bases bearing furan moieties 2. Polyazines and polyazomethines, *Polymer International*, 40 (1996) 33-39.
- [26] A.S. Amarasekara, D. Green, L.D. Williams, Renewable resources based polymers: Synthesis and characterization of 2,5-diformylfuran-urea resin, *European Polymer Journal*, 45 (2009) 595-598.
- [27] H. Choudhary, S. Nishimura, K. Ebitani, Metal-free oxidative synthesis of succinic acid from biomass-derived furan compounds using a solid acid catalyst with hydrogen peroxide, *Applied Catalysis A: General*, 458 (2013) 55-62.
- [28] S. Li, K. Su, Z. Li, B. Cheng, Selective oxidation of 5-hydroxymethylfurfural with H₂O₂ catalyzed by a molybdenum complex, *Green Chemistry*, 18 (2016) 2122-2128.
- [29] P.A. Son, S. Nishimura, K. Ebitani, Synthesis of levulinic acid from fructose using Amberlyst-15 as a solid acid catalyst, *Reaction Kinetics, Mechanisms and Catalysis*, 106 (2012) 185-192.
- [30] J. Nie, J. Xie, H. Liu, Efficient aerobic oxidation of 5-hydroxymethylfurfural to 2,5-diformylfuran on supported Ru catalysts, *Journal of Catalysis*, 301 (2013) 83-91.
- [31] M.L. Ribeiro, U. Schuchardt, Cooperative effect of cobalt acetylacetonate and silica in the catalytic cyclization and oxidation of fructose to 2,5-furandicarboxylic acid, *Catalysis Communications*, 4 (2003) 83-86.
- [32] W. Partenheimer, Vladimir V. Grushin, Synthesis of 2,5-Diformylfuran and Furan-2,5-Dicarboxylic Acid by Catalytic Air-Oxidation of 5-Hydroxymethylfurfural. Unexpectedly Selective Aerobic Oxidation of Benzyl Alcohol to Benzaldehyde with Metal=Bromide Catalysts, *Advanced Synthesis & Catalysis*, 343 (2001) 102-111.
- [33] P. Verdeguer, N. Merat, A. Gaset, Oxydation catalytique du HMF en acide 2,5-furane dicarboxylique, *Journal of Molecular Catalysis*, 85 (1993) 327-344.
- [34] M. Kröger, U. Prüße, K.-D. Vorlop, A new approach for the production of 2,5-furandicarboxylic acid by in situ oxidation of 5-hydroxymethylfurfural starting from fructose, *Topics in Catalysis*, 13 (2000) 237-242.

- [35] S.E. Davis, L.R. Houk, E.C. Tamargo, A.K. Datye, R.J. Davis, Oxidation of 5-hydroxymethylfurfural over supported Pt, Pd and Au catalysts, *Catalysis Today*, 160 (2011) 55-60.
- [36] S.E. Davis, A.D. Benavidez, R.W. Gosselink, J.H. Bitter, K.P. de Jong, A.K. Datye, R.J. Davis, Kinetics and mechanism of 5-hydroxymethylfurfural oxidation and their implications for catalyst development, *Journal of Molecular Catalysis A: Chemical*, 388–389 (2014) 123-132.
- [37] R. Sahu, P.L. Dhepe, Synthesis of 2,5-furandicarboxylic acid by the aerobic oxidation of 5-hydroxymethyl furfural over supported metal catalysts, *Reaction Kinetics, Mechanisms and Catalysis*, 112 (2014) 173-187.
- [38] S. Siankevich, G. Savoglidis, Z. Fei, G. Laurenczy, D.T.L. Alexander, N. Yan, P.J. Dyson, A novel platinum nanocatalyst for the oxidation of 5-Hydroxymethylfurfural into 2,5-Furandicarboxylic acid under mild conditions, *Journal of Catalysis*, 315 (2014) 67-74.
- [39] B. Siyo, M. Schneider, M.-M. Pohl, P. Langer, N. Steinfeldt, Synthesis, Characterization, and Application of PVP-Pd NP in the Aerobic Oxidation of 5-Hydroxymethylfurfural (HMF), *Catalysis Letters*, 144 (2014) 498-506.
- [40] B. Siyo, M. Schneider, J. Radnik, M.-M. Pohl, P. Langer, N. Steinfeldt, Influence of support on the aerobic oxidation of HMF into FDCA over preformed Pd nanoparticle based materials, *Applied Catalysis A: General*, 478 (2014) 107-116.
- [41] N. Mei, B. Liu, J. Zheng, K. Lv, D. Tang, Z. Zhang, A novel magnetic palladium catalyst for the mild aerobic oxidation of 5-hydroxymethylfurfural into 2,5-furandicarboxylic acid in water, *Catalysis Science & Technology*, 5 (2015) 3194-3202.
- [42] C.A. Antonyraj, J. Jeong, B. Kim, S. Shin, S. Kim, K.-Y. Lee, J.K. Cho, Selective oxidation of HMF to DFF using Ru/ γ -alumina catalyst in moderate boiling solvents toward industrial production, *Journal of Industrial and Engineering Chemistry*, 19 (2013) 1056-1059.
- [43] P. Gamez, I.W.C.E. Arends, R.A. Sheldon, J. Reedijk, Room Temperature Aerobic Copper-Catalysed Selective Oxidation of Primary Alcohols to Aldehydes, *Advanced Synthesis & Catalysis*, 346 (2004) 805-811.
- [44] T.S. Hansen, I. Sádaba, E.J. García-Suárez, A. Riisager, Cu catalyzed oxidation of 5-hydroxymethylfurfural to 2,5-diformylfuran and 2,5-furandicarboxylic acid under benign reaction conditions, *Applied Catalysis A: General*, 456 (2013) 44-50.
- [45] A.S. Amarasekara, D. Green, E. McMillan, Efficient oxidation of 5-hydroxymethylfurfural to 2,5-diformylfuran using Mn(III)-salen catalysts, *Catalysis Communications*, 9 (2008) 286-288.
- [46] F. Rajabi, A.M. Balu, F. Toreinia, R. Luque, A versatile supported cobalt(ii) complex for heterogeneously catalysed processes: conventional vs. microwave irradiation protocols, *Catalysis Science & Technology*, 1 (2011) 1051-1059.
- [47] F. Rajabi, R. Luque, J.H. Clark, B. Karimi, D.J. Macquarrie, A silica supported cobalt (II) Salen complex as efficient and reusable catalyst for the selective aerobic oxidation of ethyl benzene derivatives, *Catalysis Communications*, 12 (2011) 510-513.
- [48] Y. Yang, Y. Zhang, S. Hao, Q. Kan, Tethering of Cu(II), Co(II) and Fe(III) tetrahydro-salen and salen complexes onto amino-functionalized SBA-15: Effects of salen ligand hydrogenation on catalytic performances for aerobic epoxidation of styrene, *Chemical Engineering Journal*, 171 (2011) 1356-1366.

- [49] P. Karandikar, M. Agashe, K. Vijayamohanan, A.J. Chandwadkar, Cu²⁺-perchlorophthalocyanine immobilized MCM-41: catalyst for oxidation of alkenes, *Applied Catalysis A: General*, 257 (2004) 133-143.
- [50] X.-G. Zhou, X.-Q. Yu, J.-S. Huang, C.-M. Che, S.-G. Li, L.-S. Li, Asymmetric epoxidation of alkenes catalysed by chromium binaphthyl Schiff base complex supported on MCM-41, *Chemical Communications*, (1999) 1789-1790.
- [51] C.K.P. Neeli, S. Ganji, V.S.P. Ganjala, S.R.R. Kamaraju, D.R. Burri, Oxidative coupling of primary amines to imines under base-free and additive-free conditions over AuNPs/SBA-NH₂ nanocatalyst, *RSC Advances*, 4 (2014) 14128-14135.
- [52] P. Karandikar, K.C. Dhanya, S. Deshpande, A.J. Chandwadkar, S. Sivasanker, M. Agashe, Cu/Co-salen immobilized MCM-41: characterization and catalytic reactions, *Catalysis Communications*, 5 (2004) 69-74.
- [53] S.K. Badamali, R. Luque, J.H. Clark, S.W. Breeden, Microwave assisted oxidation of a lignin model phenolic monomer using Co(salen)/SBA-15, *Catalysis Communications*, 10 (2009) 1010-1013.
- [54] C. Li-Juan, M. Fu-Ming, L. Guang-Xing, Co(II) Schiff base complexes on silica by sol-gel method as heterogeneous catalysts for oxidative carbonylation of aniline, *Catalysis Communications*, 10 (2009) 981-985.
- [55] R. Ji, K. Yu, L.-L. Lou, S. Liu, Reactivity comparison of epoxidation of unfunctionalized olefins with different oxidants catalyzed by mesoporous silica supported unsymmetric chiral Mn(III) salen complexes in heterogeneous condition, *Journal of Molecular Catalysis A: Chemical*, 378 (2013) 7-16.
- [56] X. Chen, N. Xu, N. Li, L. Lu, Y. Cai, Y. Zhao, D. Wang, Programmable selectivity of metal-imine bond coordination in subcomponent self-assembly of a primary amine based block copolymer, *Soft Matter*, 9 (2013) 1885-1894.
- [57] Y. Yang, S. Hao, P. Qiu, F. Shang, W. Ding, Q. Kan, A novel copper(II) complex bearing salicylaldimine immobilized on SBA-15 and its catalytic performances in styrene oxidation by hydrogen peroxide, *Reaction Kinetics, Mechanisms and Catalysis*, 100 (2010) 363-375.
- [58] V.D. Chaube, S. Shylesh, A.P. Singh, Synthesis, characterization and catalytic activity of Mn(III)- and Co(II)-salen complexes immobilized mesoporous alumina, *Journal of Molecular Catalysis A: Chemical*, 241 (2005) 79-87.
- [59] L. Ma, F. Su, X. Zhang, D. Song, Y. Guo, J. Hu, Epoxidation of alkenes catalyzed by highly ordered mesoporous manganese-salen-based hybrid catalysts, *Microporous and Mesoporous Materials*, 184 (2014) 37-46.
- [60] M. Salavati-Niasari, M. Bazarganipour, Synthesis, characterization and catalytic oxidation properties of multi-wall carbon nanotubes with a covalently attached copper(II) salen complex, *Applied Surface Science*, 255 (2009) 7610-7617.
- [61] T. Kurahashi, H. Fujii, Unique Ligand-Radical Character of an Activated Cobalt Salen Catalyst That Is Generated by Aerobic Oxidation of a Cobalt(II) Salen Complex, *Inorganic Chemistry*, 52 (2013) 3908-3919.
- [62] D.J. Darensbourg, C.G. Ortiz, D.R. Billodeaux, Synthesis and structural characterization of iron(III) salen complexes possessing appended anionic oxygen donor ligands, *Inorganica Chimica Acta*, 357 (2004) 2143-2149.
- [63] D.P. Serrano, J. Aguado, C. Vargas, A comparison of methods for the heterogenization of the chiral Jacobsen catalyst on mesostructured SBA-15 supports, *Applied Catalysis A: General*, 335 (2008) 172-179.

- [64] J. Nakazawa, B.J. Smith, T.D.P. Stack, Discrete Complexes Immobilized onto Click-SBA-15 Silica: Controllable Loadings and the Impact of Surface Coverage on Catalysis, *Journal of the American Chemical Society*, 134 (2012) 2750-2759.
- [65] K.S.W. Sing, D.H. Everett, R.A.W. Haul, L. Moscou, R.A. Pierotti, J. Rouquerol, T. Siemieniewska, Reporting Physisorption Data for Gas/Solid Systems, *Handbook of Heterogeneous Catalysis*, Wiley-VCH Verlag GmbH & Co. KGaA2008.
- [66] D.X. Martínez Vargas, J. Rivera De la Rosa, C.J. Lucio-Ortiz, A. Hernández-Ramirez, G.A. Flores-Escamilla, C.D. Garcia, Photocatalytic degradation of trichloroethylene in a continuous annular reactor using Cu-doped TiO₂ catalysts by sol-gel synthesis, *Applied Catalysis B: Environmental*, 179 (2015) 249-261.
- [67] R. Luque, S.K. Badamali, J.H. Clark, M. Fleming, D.J. Macquarrie, Controlling selectivity in catalysis: Selective greener oxidation of cyclohexene under microwave conditions, *Applied Catalysis A: General*, 341 (2008) 154-159.
- [68] N. Anand, K.H.P. Reddy, V. Swapna, K.S.R. Rao, D.R. Burri, Fe(III) complex anchored SBA-15 is a new heterogeneous catalyst for the cleavage of aliphatic CC bond of styrene and its derivatives, *Microporous and Mesoporous Materials*, 143 (2011) 132-140.
- [69] Z. Chen, F. Shan, L. Cao, G. Fang, Synthesis and thermal properties of shape-stabilized lauric acid/activated carbon composites as phase change materials for thermal energy storage, *Solar Energy Materials and Solar Cells*, 102 (2012) 131-136.
- [70] J. Fonseca, J. Tedim, K. Biernacki, A.L. Magalhães, S.J. Gurman, C. Freire, A.R. Hillman, Structural and electrochemical characterisation of [Pd(salen)]-type conducting polymer films, *Electrochimica Acta*, 55 (2010) 7726-7736.
- [71] E.V. Alekseeva, I.A. Chepurnaya, V.V. Malev, A.M. Timonov, O.V. Levin, Polymeric nickel complexes with salen-type ligands for modification of supercapacitor electrodes: impedance studies of charge transfer and storage properties, *Electrochimica Acta*.
- [72] T. Okada, N. Arimura, C. Ono, M. Yuasa, Electro-oxidation of methanol on mixed catalysts based on platinum and organic metal complexes in acidic media, *Electrochimica Acta*, 51 (2005) 1130-1139.
- [73] Y. Yang, S. Hao, Y. Zhang, Q. Kan, Oxovanadium(IV) and dioxomolybdenum(VI) salen complexes tethered onto amino-functionalized SBA-15 for the epoxidation of cyclooctene, *Solid State Sciences*, 13 (2011) 1938-1942.
- [74] M. Salavati-Niasari, S.N. Mirsattari, M. Bazarganipour, Synthesis, characterization and catalytic oxyfunctionalization of cyclohexene with tert-butylhydroperoxide over a manganese(II) complex covalently anchored to multi-wall carbon nanotubes (MWNTs), *Polyhedron*, 27 (2008) 3653-3661.
- [75] A. De Stefanis, S. Kaciulis, L. Pandolfi, Preparation and characterization of Fe-MCM-41 catalysts employed in the degradation of plastic materials, *Microporous and Mesoporous Materials*, 99 (2007) 140-148.
- [76] J. Sun, J. Zhang, L. Wang, L. Zhu, X. Meng, F.-S. Xiao, Co-salen functionalized on graphene as an efficient heterogeneous catalyst for cyclohexene oxidation, *Journal of Energy Chemistry*, 22 (2013) 48-51.
- [77] X. Zhou, P. Xu, L. Xu, Z. Bai, Z. Chen, J. Qiao, J. Zhang, N,N'-Bis(salicylidene)ethylenediamine as a nitrogen-rich precursor to synthesize electrocatalysts with high methanol-tolerance for polymer electrolyte membrane fuel cell oxygen reduction reaction, *Journal of Power Sources*, 260 (2014) 349-356.

- [78] V.S. Kshirsagar, A.C. Garade, R.B. Mane, K.R. Patil, A. Yamaguchi, M. Shirai, C.V. Rode, Characterization of clay intercalated cobalt-salen catalysts for the oxidation of p-cresol, *Applied Catalysis A: General*, 370 (2009) 16-23.
- [79] T. Yamashita, P. Hayes, Analysis of XPS spectra of Fe²⁺ and Fe³⁺ ions in oxide materials, *Applied Surface Science*, 254 (2008) 2441-2449.
- [80] P. Bruggeller, E. Mayer, Complete vitrification in pure liquid water and dilute aqueous solutions, *Nature*, 288 (1980) 569-571.
- [81] Lj. Kundakovic, M. Flytzani-Stephanopoulos, Reduction characteristics of copper oxide in cerium and zirconium oxide systems, *Applied Catalysis A: General* 171 (1998) 13-29.
- [82] M. Toshiro, Copper Oxide Thin Films Prepared from Copper Dipivaloylmethanate and Oxygen by Chemical Vapor Deposition, *Japanese Journal of Applied Physics*, 37 (1998) 4099.
- [83] W. Li, Z. Zhang, J. Wang, W. Qiao, D. Long, L. Ling, Low temperature catalytic combustion of ethylene over cobalt oxide supported mesoporous carbon spheres, *Chemical Engineering Journal*, 293 (2016) 243-251.
- [84] S. Wang, B. Zhang, C. Zhao, S. Li, M. Zhang, L. Yan, Valence control of cobalt oxide thin films by annealing atmosphere, *Applied Surface Science*, 257 (2011) 3358-3362.
- [85] O. Levenspiel, *Chemical reaction engineering in: J.W. Sons (Ed.), 1999, pp. 668.*

Fig. 1. Diagram of the metal Salen complex catalyst synthesis (Cu Salen/SBA-15).

Fig. 2. FTIR spectra of SBA-15 (a), Fe Salen/SBA-15 (b), Cu Salen/SBA-15 (c) and Co Salen/SBA-15 (d). The dotted line refers to the band at 1063 cm^{-1} showed for all the spectra.

Fig. 3. Monitoring the imine synthesis for the formation of metal complexes by UV-Vis spectra. Where 3-aminopropyltriethoxysilano (APTES) (a), salicylaldehyde (b), salicylaldehyde-APTES (c), salicylaldehyde-APTES after 3 h stirring (d).

Fig. 4. UV-vis spectra of the metal Salen complex Fe Salen (a), Cu Salen (b) y Co Salen (c); where dot lines are from the samples taken after 3 h stirring and solid lines after additional 15 h stirring.

Fig. 5. DR-UV-vis spectrums of the Fe (a), Cu (b) and Co (c) Salen complex supported on SBA-15 and the pure support (d).

Fig. 6. Nitrogen adsorption (solid symbols)/desorption (empty symbols) isotherms of Cu (a), Co (b) and Fe (c) Salen complex supported on SBA-15 and the pure support SBA-15 (d).

Fig. 7. Pore size distribution of SBA-15 and the different catalysts.

Fig. 8. Micrograph of SBA-15 showing the hexagonal channels.

Fig. 9 C1s, N1s and O1s high resolution XPS spectrums of Co Salen (a), Cu Salen (b) and Fe Salen (c) supported on SBA-15.

Fig. 10 Co 2p, Cu 2p and Fe 2p high resolution XPS spectrums of Co Salen/SBA-15 (a), Cu Salen/SBA-15 (b) and Fe Salen/SBA-15 (c) respectively.

Fig. 11. Effect of the transition metal of the catalyst.

Fig. 12. Effect of the H_2O_2 amount.

Fig. 13. Effect of the temperature. Initial HMF concentration of 0.4 mM, 100 μL of H_2O_2 30 w/V % and 0.050 g of Cu Salen/SBA-15 catalyst.

Fig. 14. Concentration versus time curves of the HMF oxidation reaction.

Fig. 15. Mechanism proposed for the formation of the identified products.

Fig. 16. First fit to the concentration versus time HMF oxidation data.

Fig. 17. Scheme of HMF oxidation through ring rupture and by oxidation of the alcohol and aldehyde sides of HMF molecule in aqueous solution.

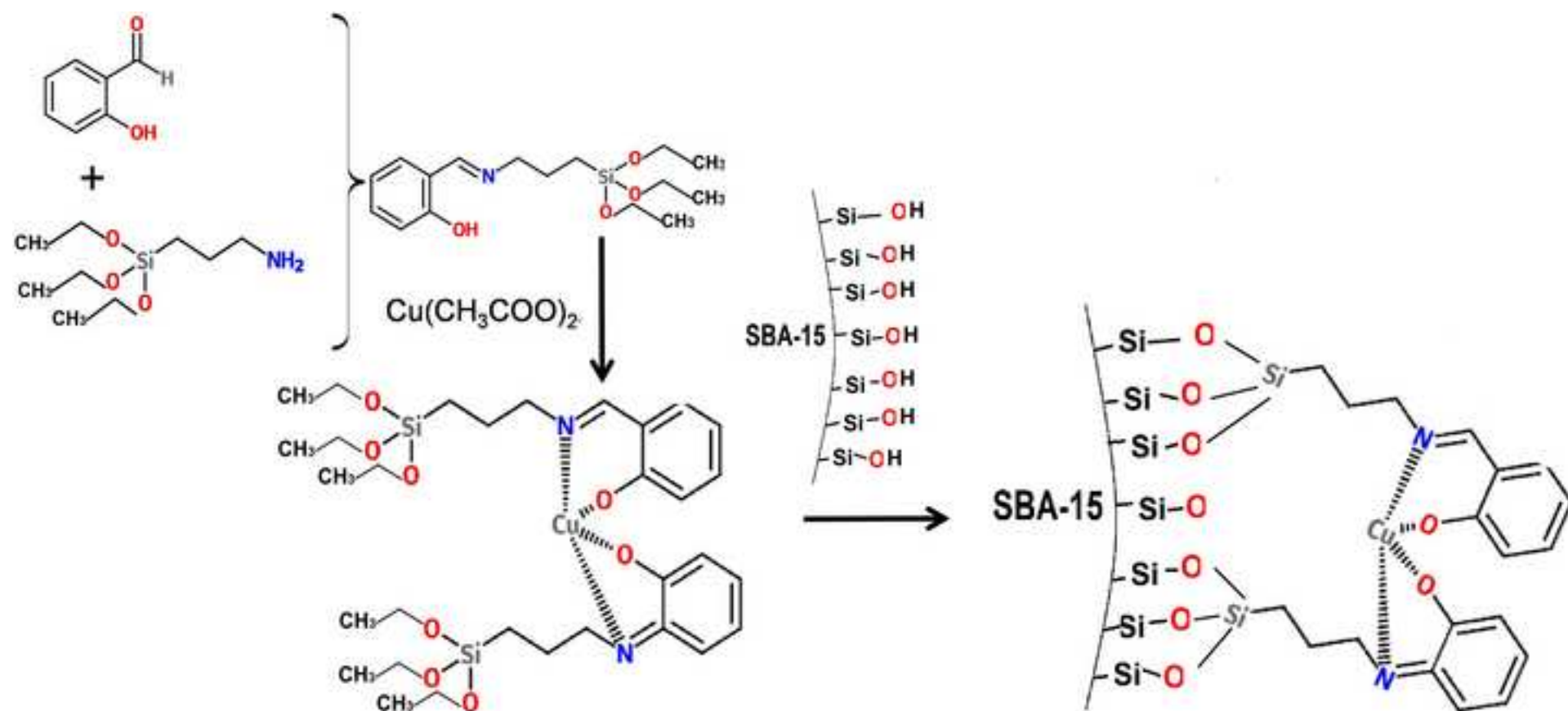
Fig. 18. Proposed mechanism of HMF oxidation step by step through oxidation of the alcohol side of HMF molecule.

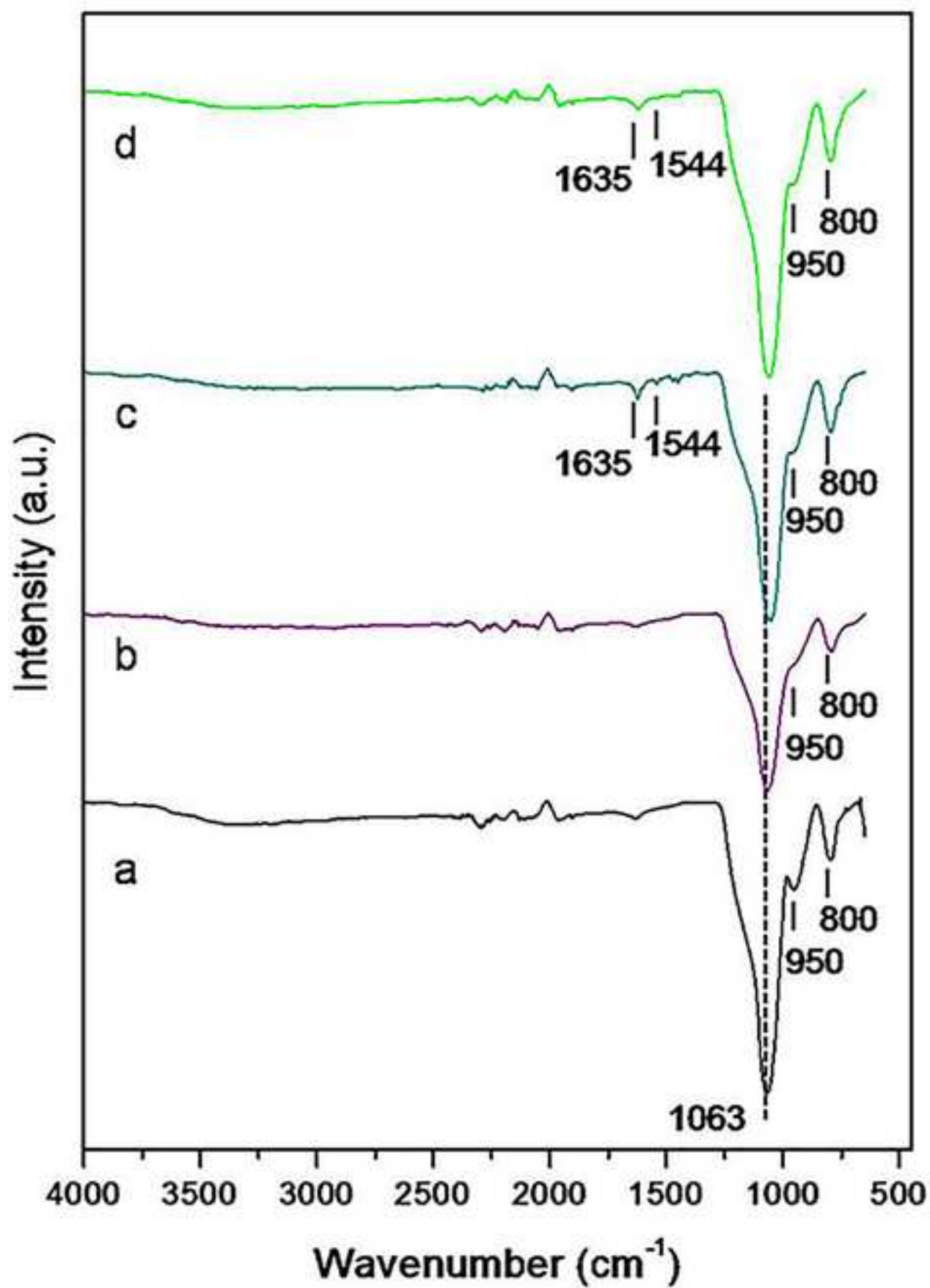
Fig. 19. Proposed mechanism of HMF oxidation step by step through oxidation of the aldehyde side of HMF molecule.

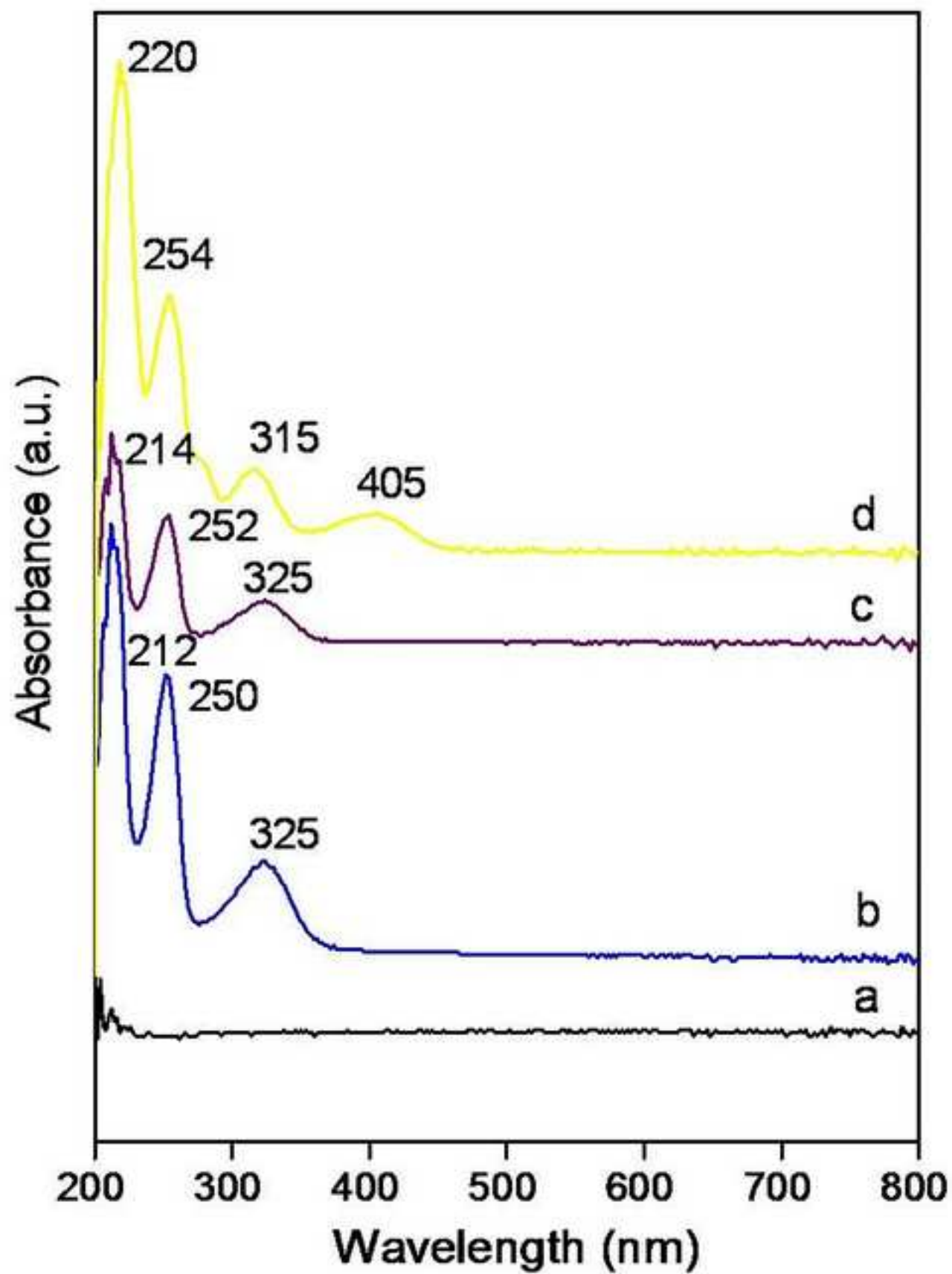
Fig. 20. Recycle test results of the Cu (II) Salen/SBA-15 catalyst.

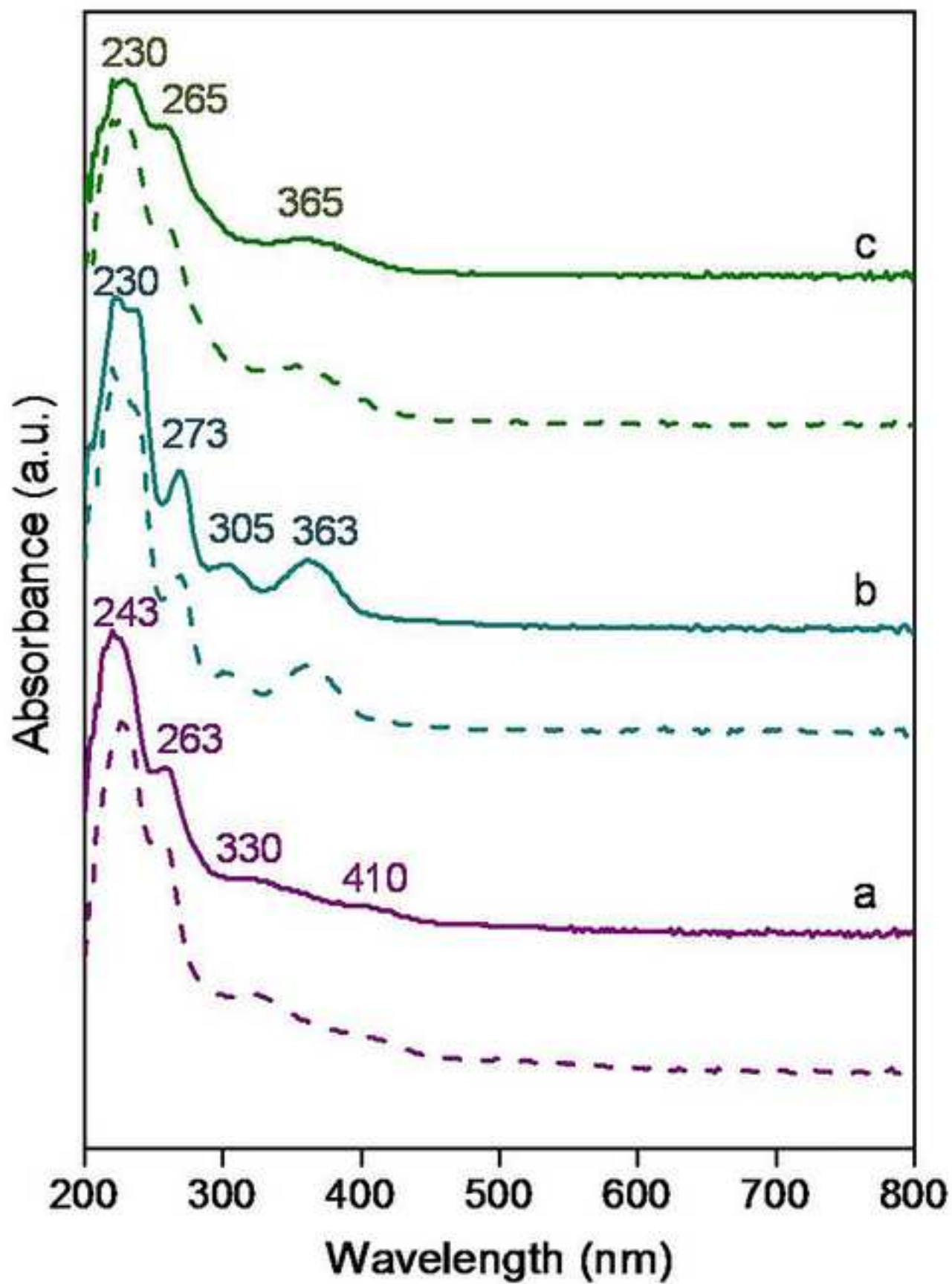
Fig. 21. DR-UV-vis spectrums of SBA-15 (a), Cu Salen/SBA-15 before (b) and after (c) being used in the reaction.

Figure 1









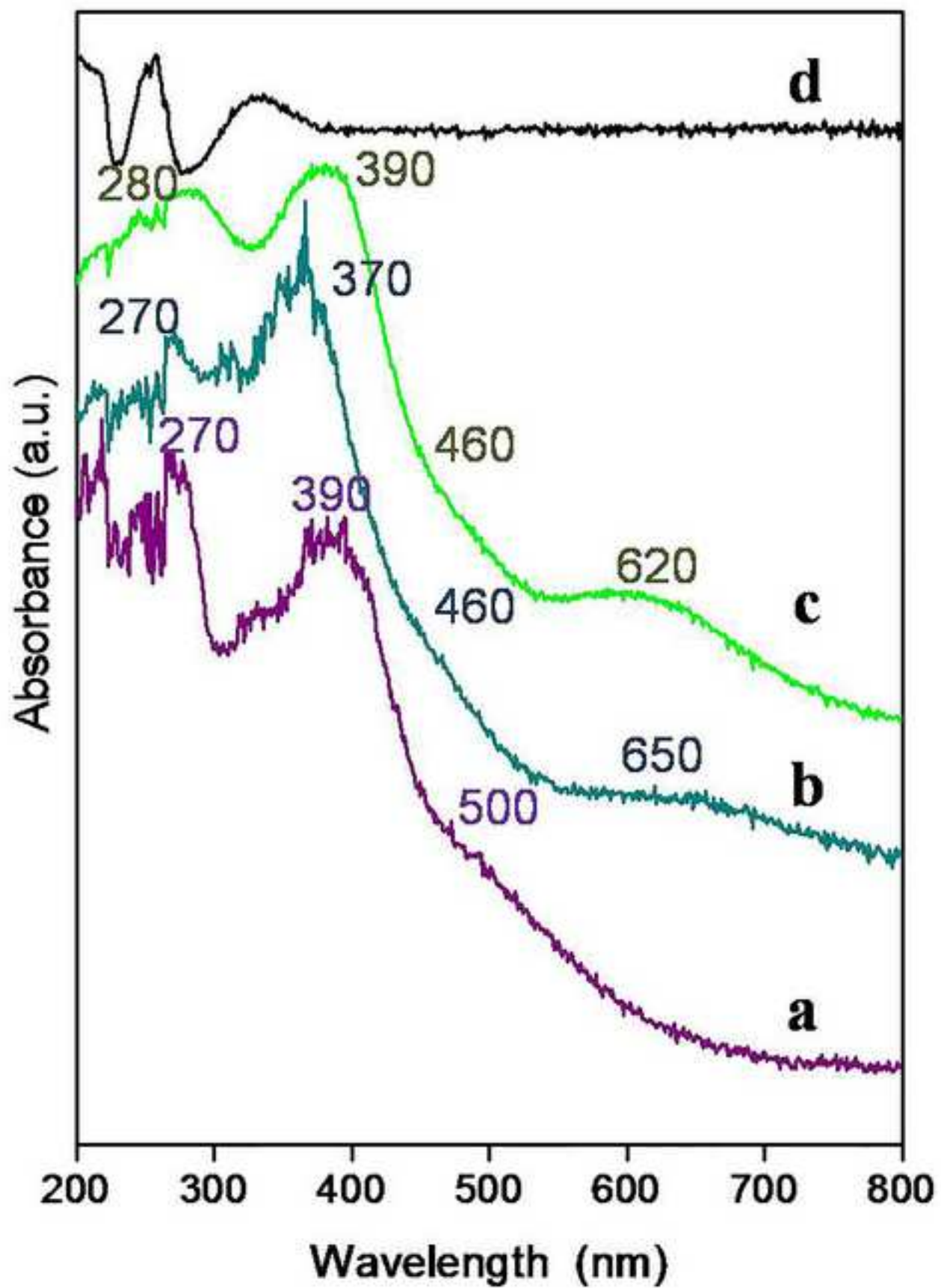


Figure 6

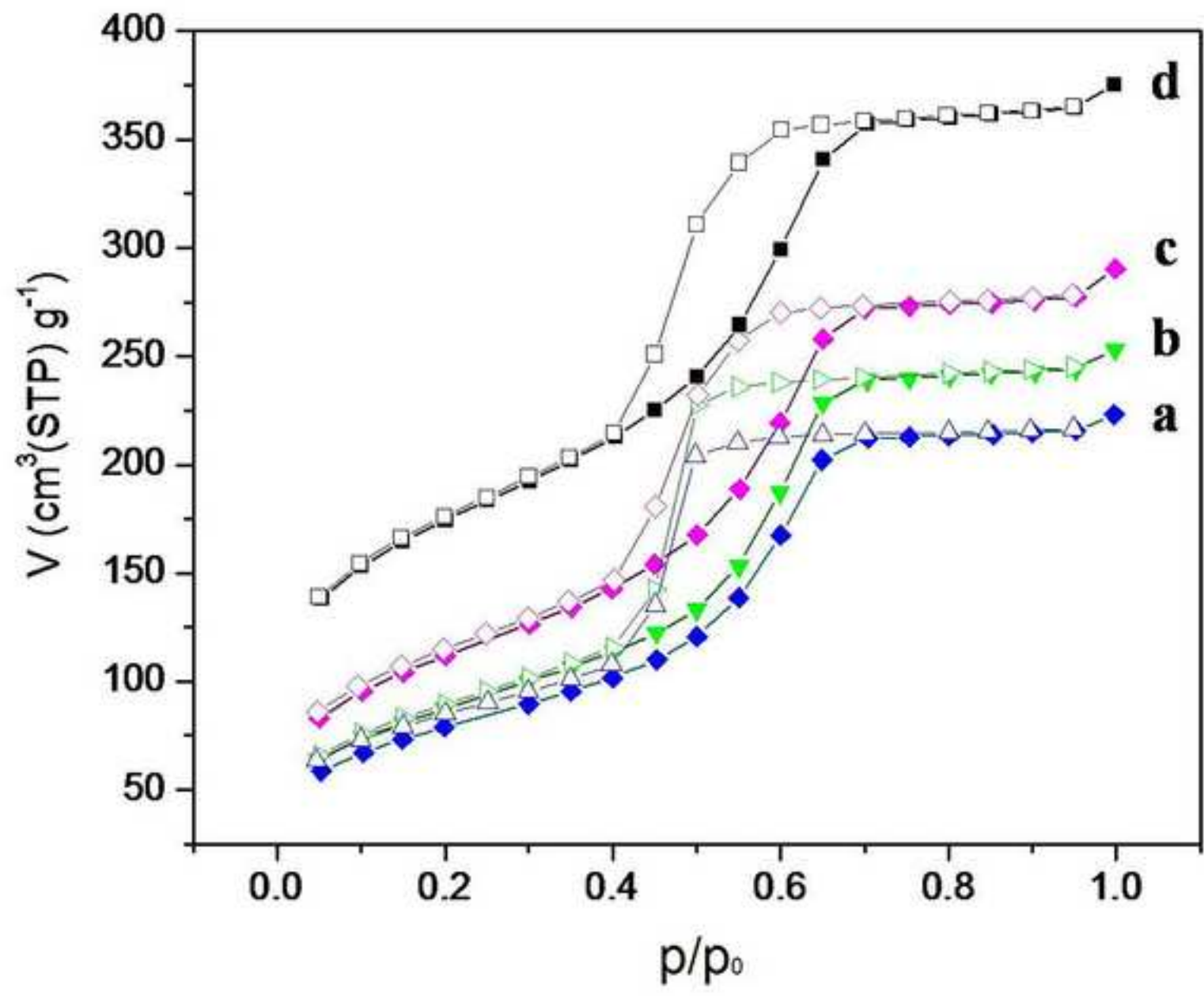


Figure 7

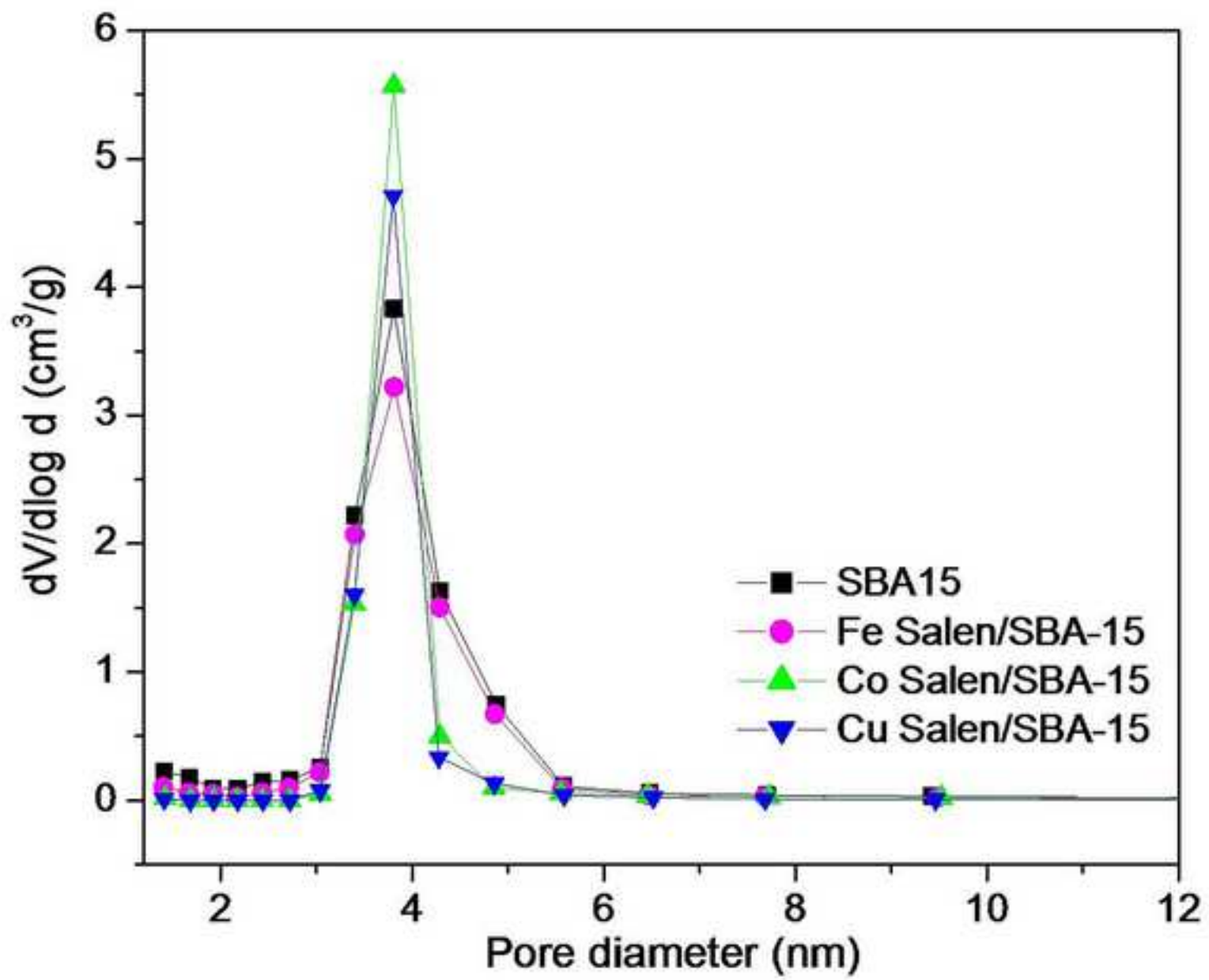


Figure 8

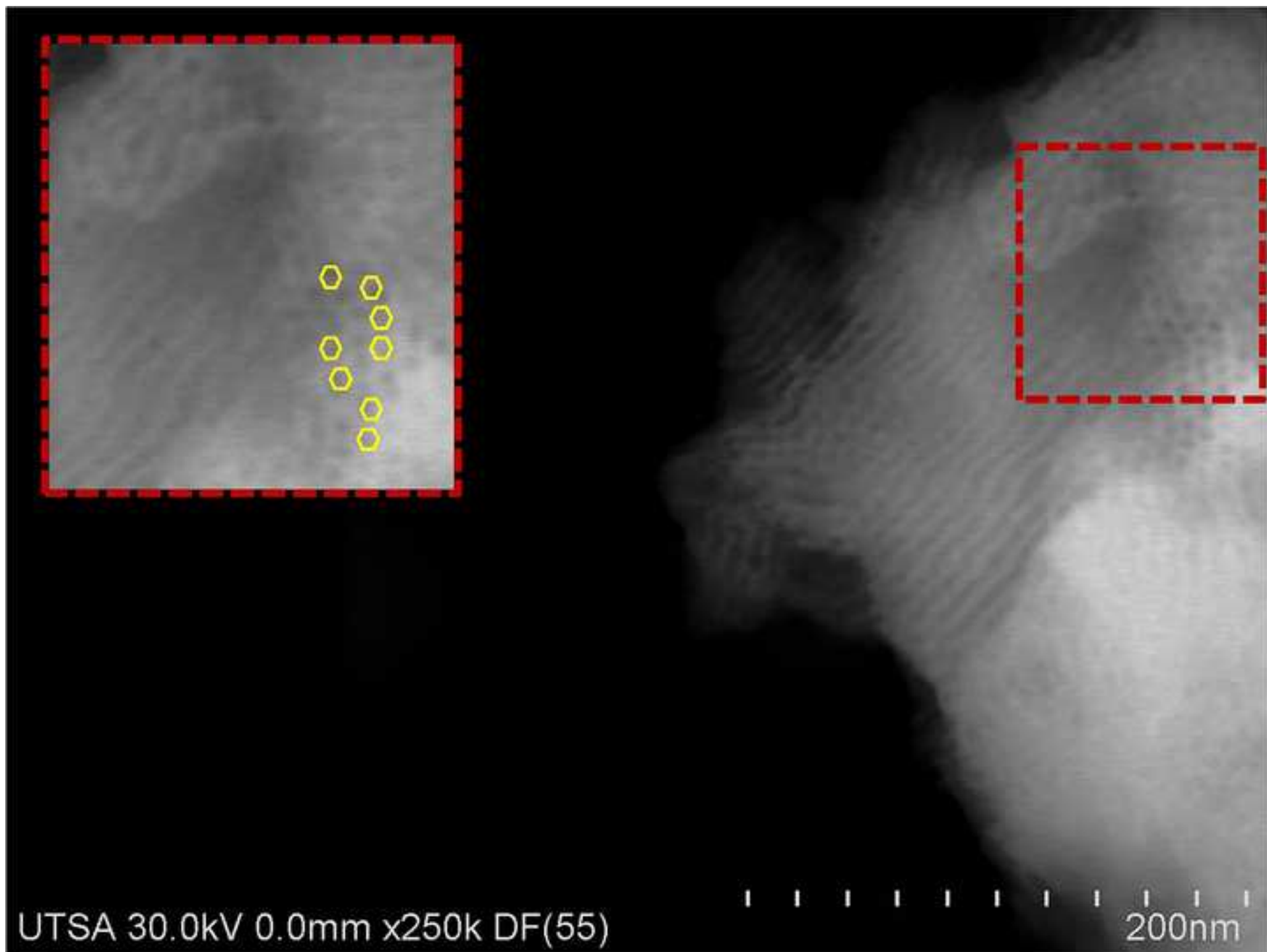
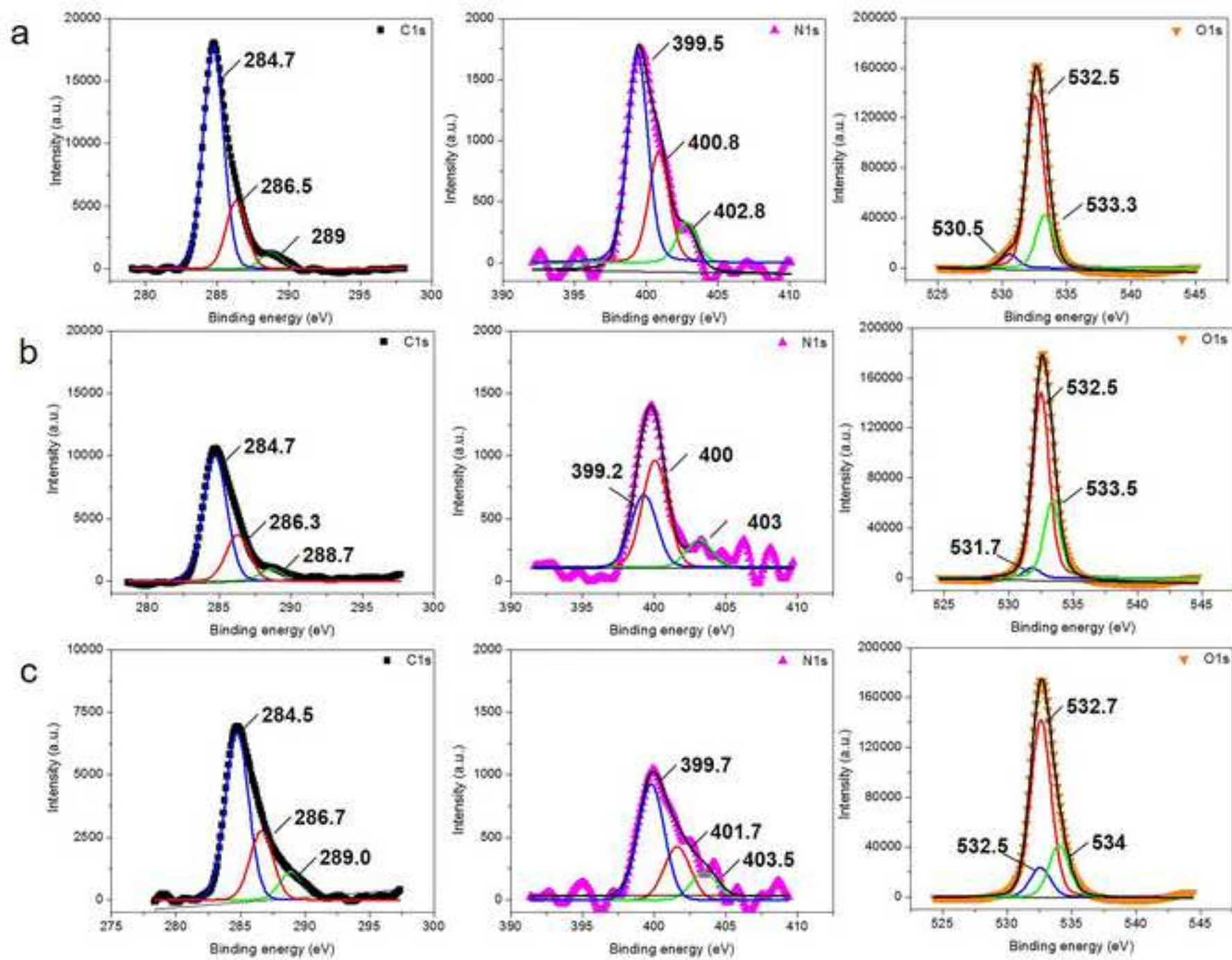


Figure 9



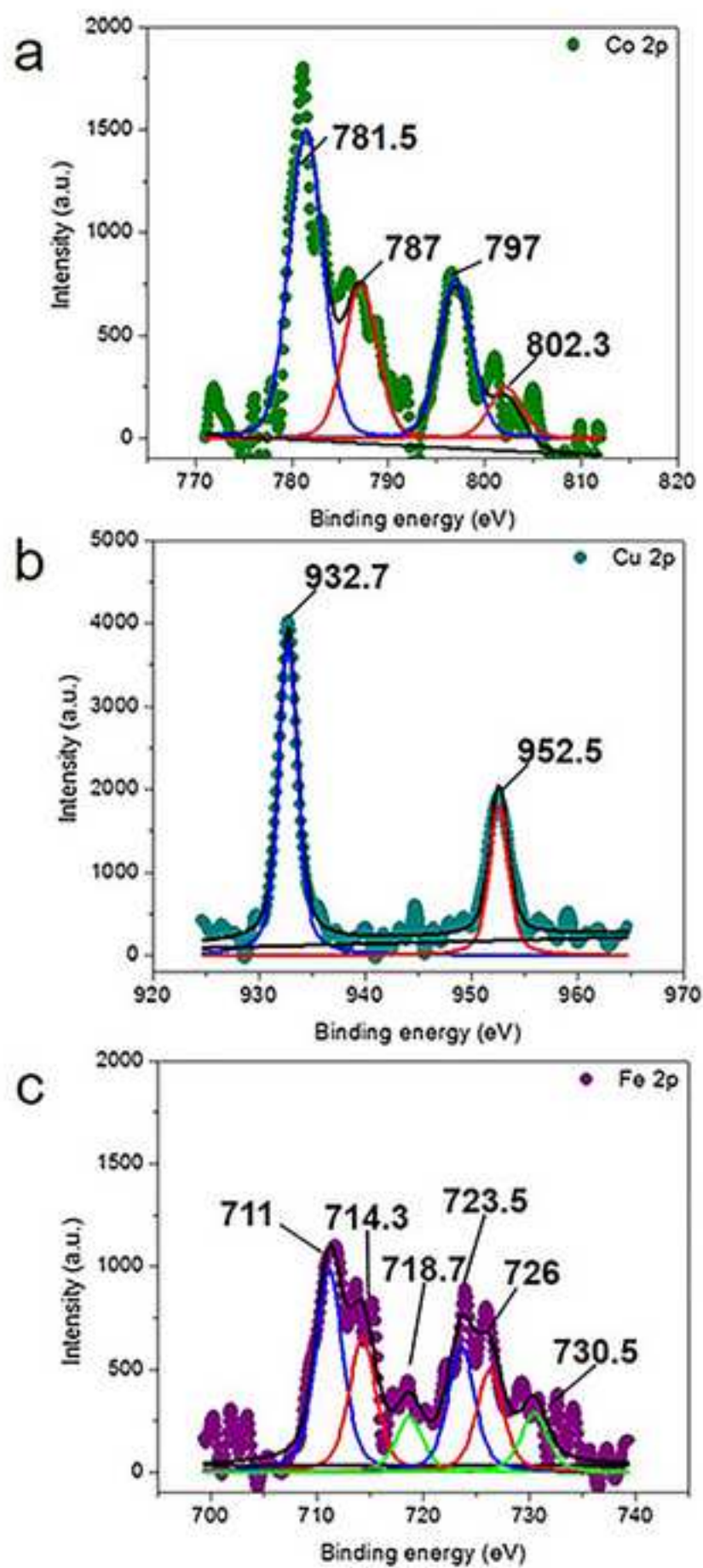


Figure 11

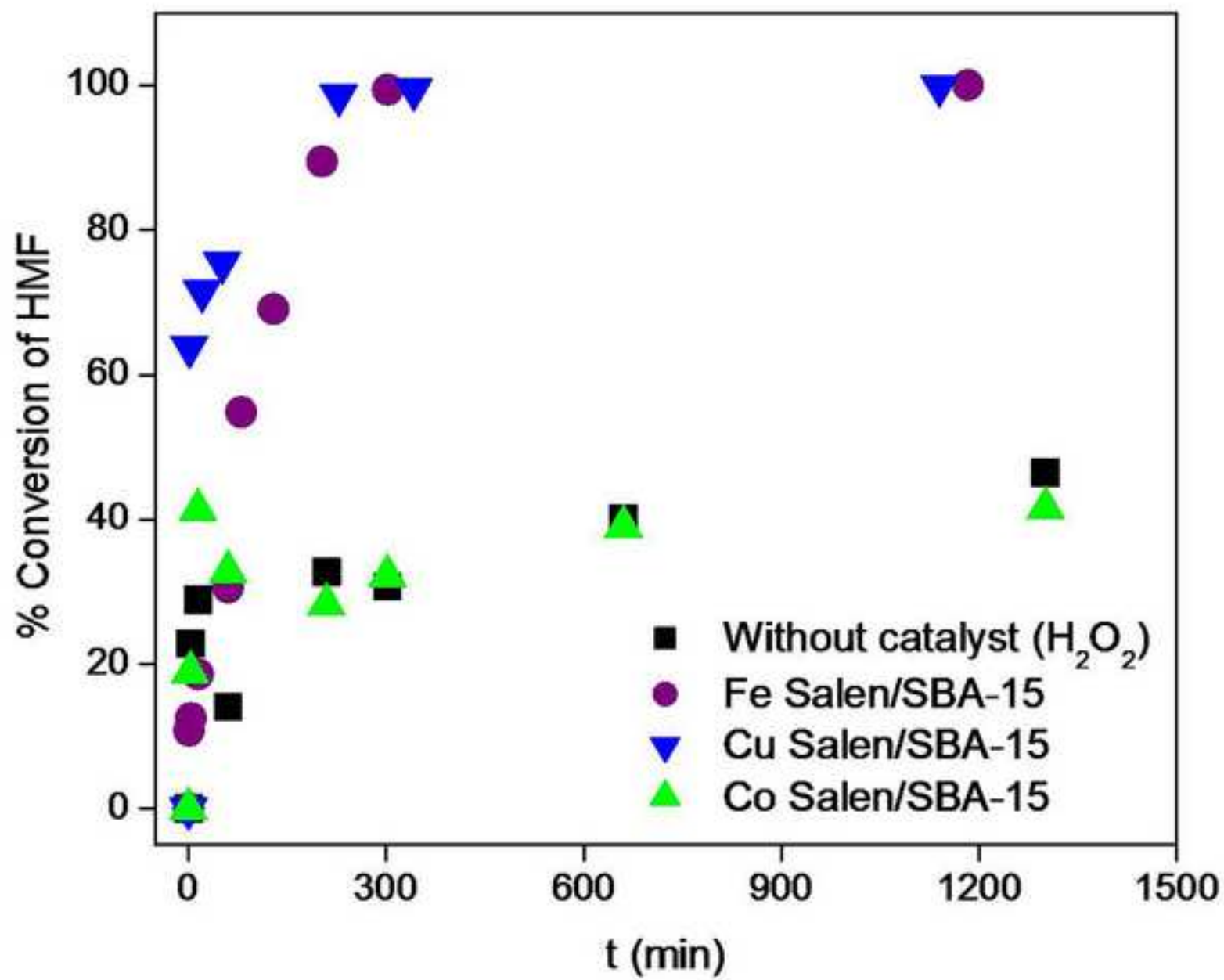


Figure 12

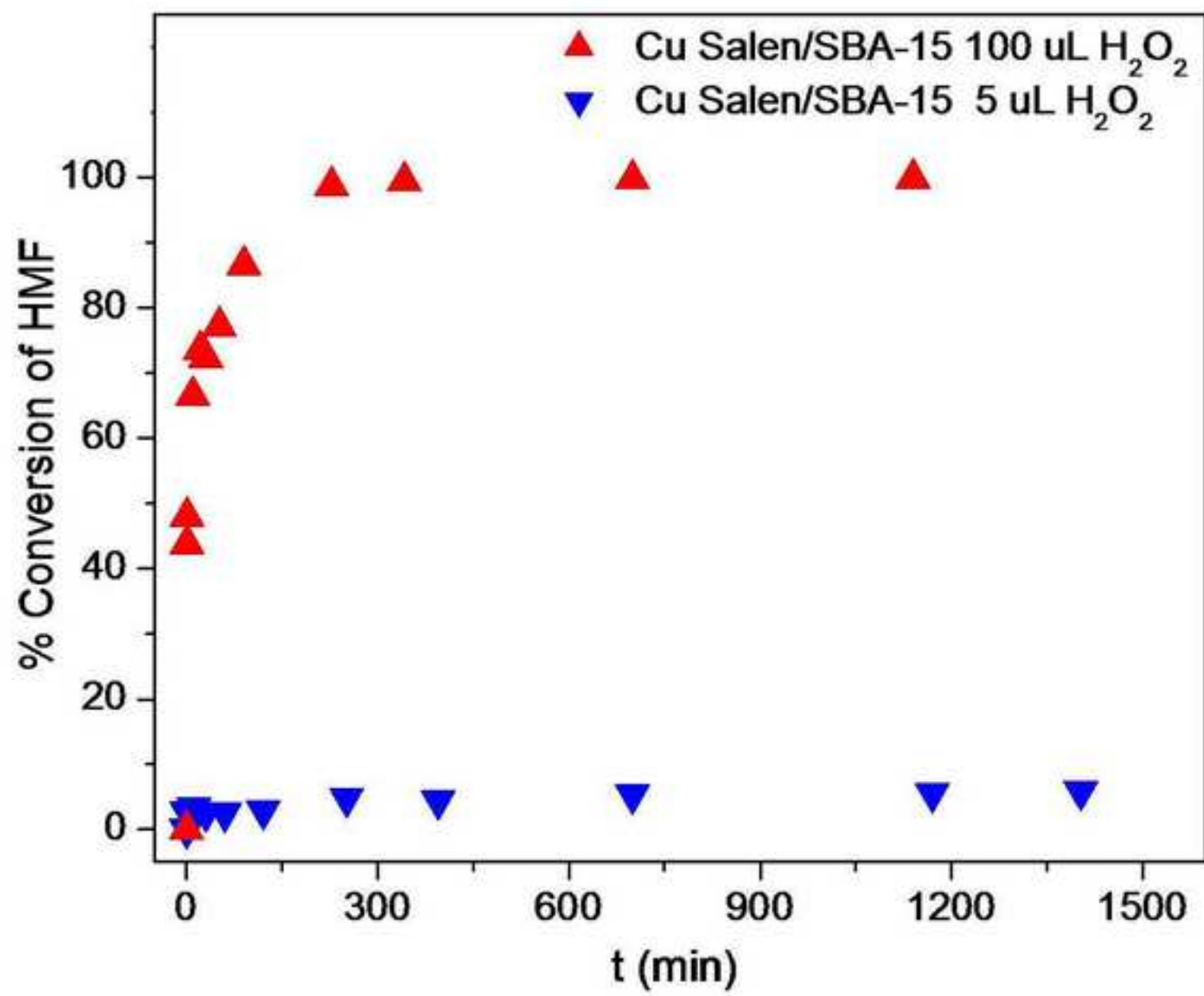


Figure 13

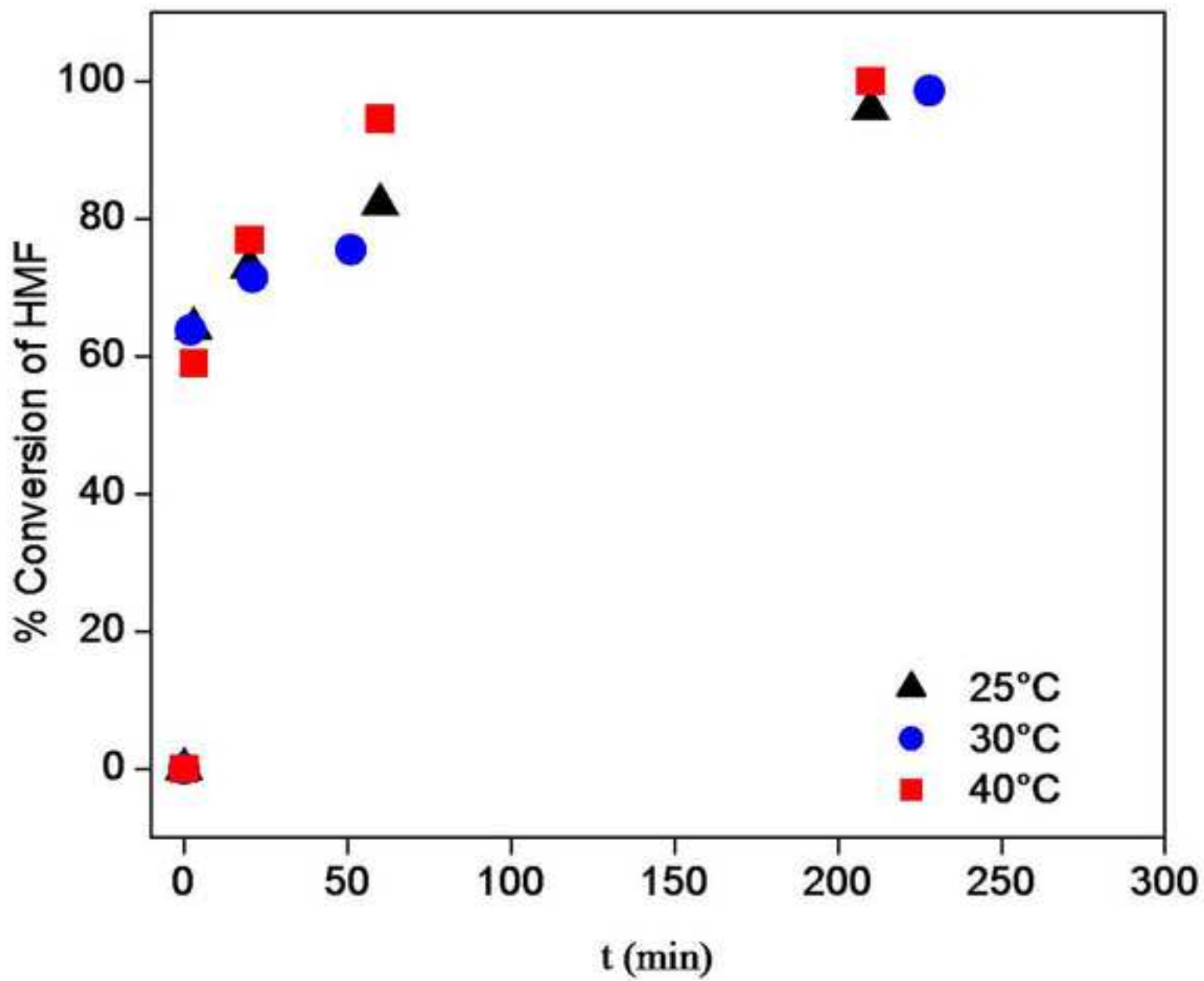


Figure 14

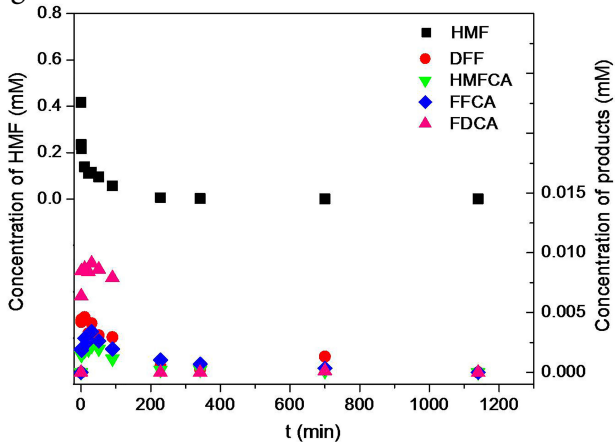


Figure 15

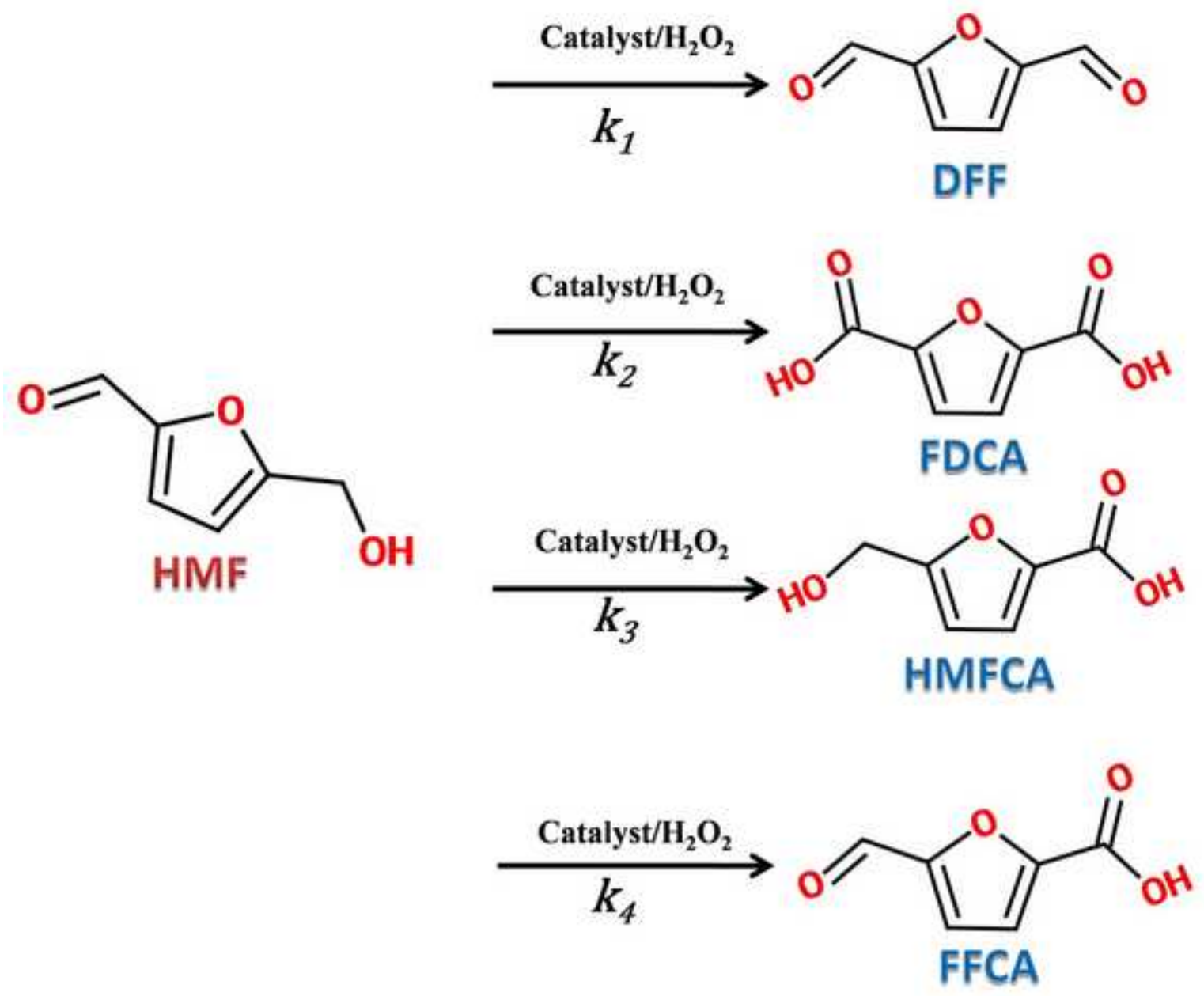


Figure 16

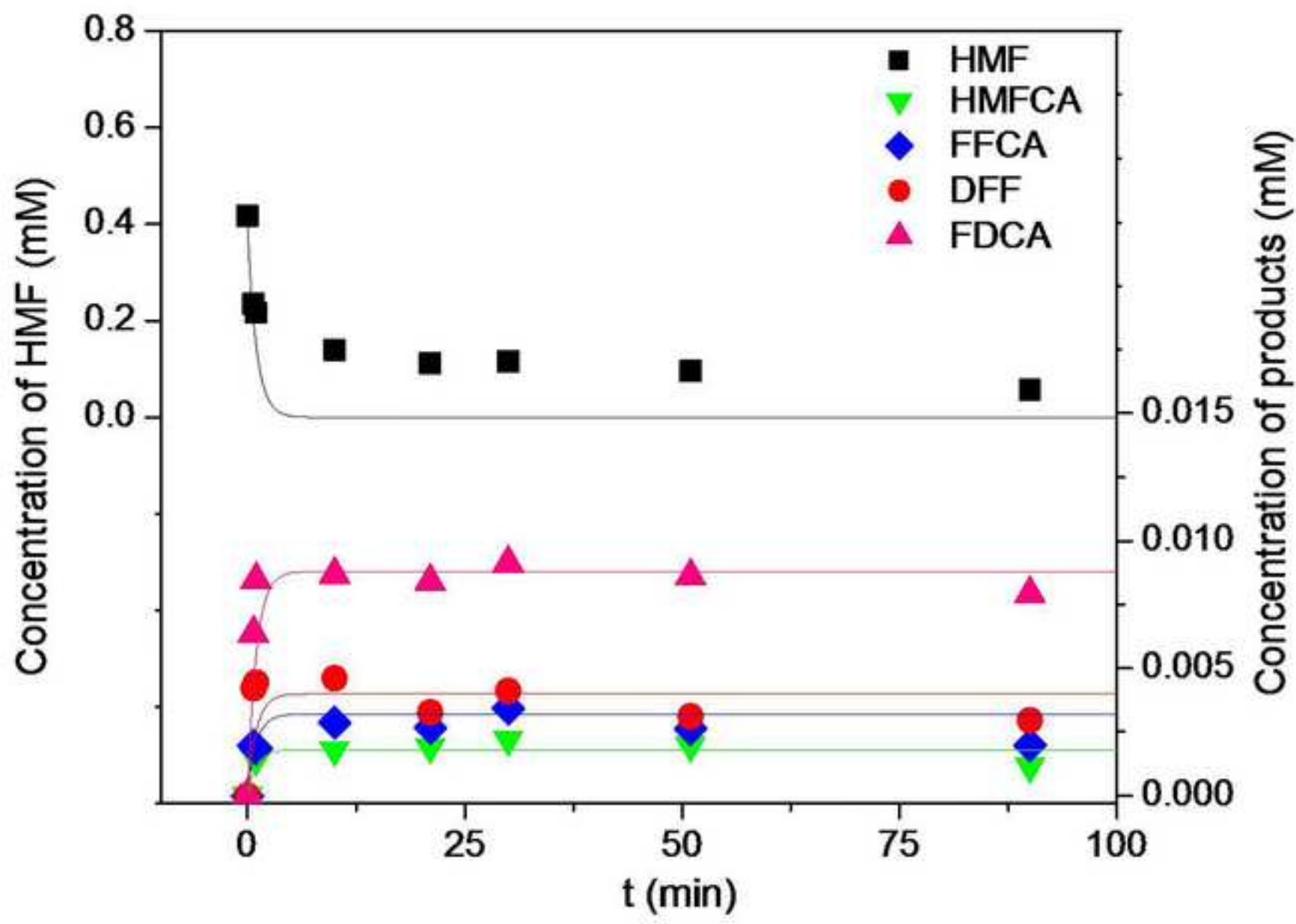


Figure 17

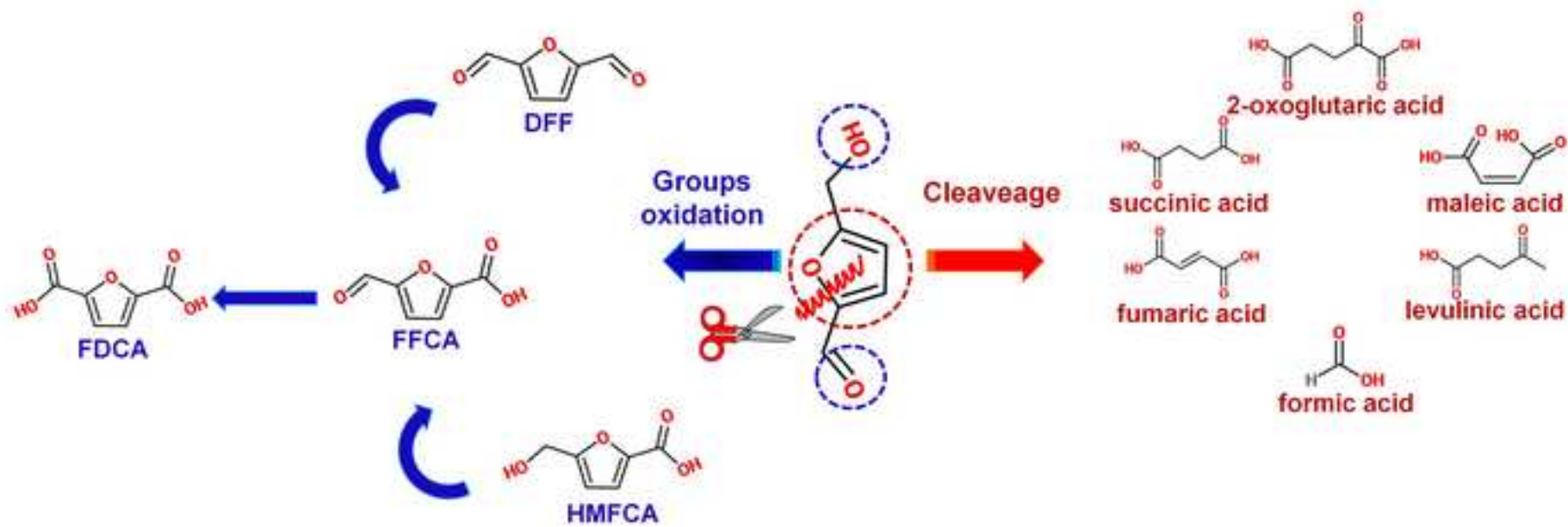


Figure 18

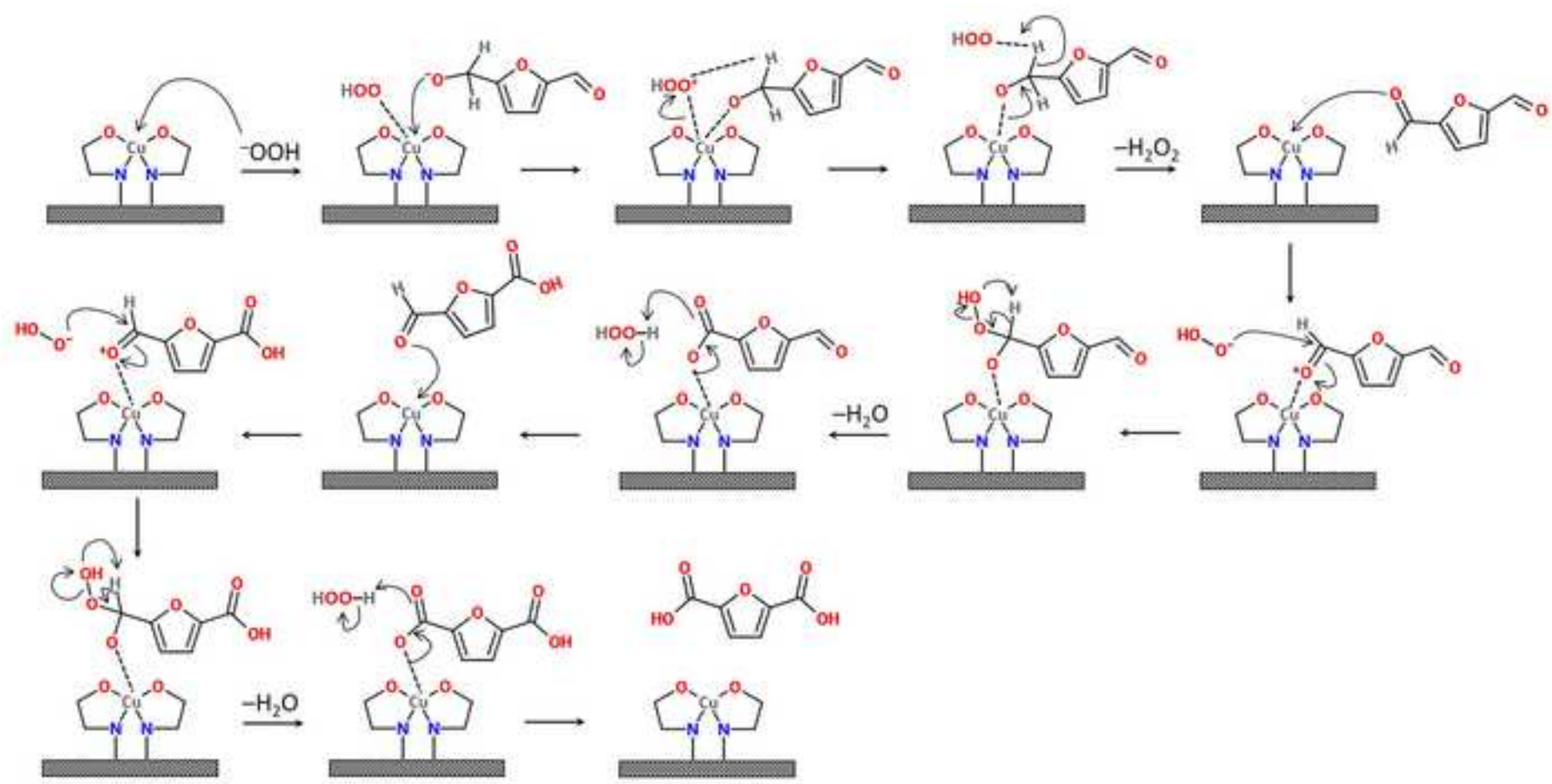


Figure 19

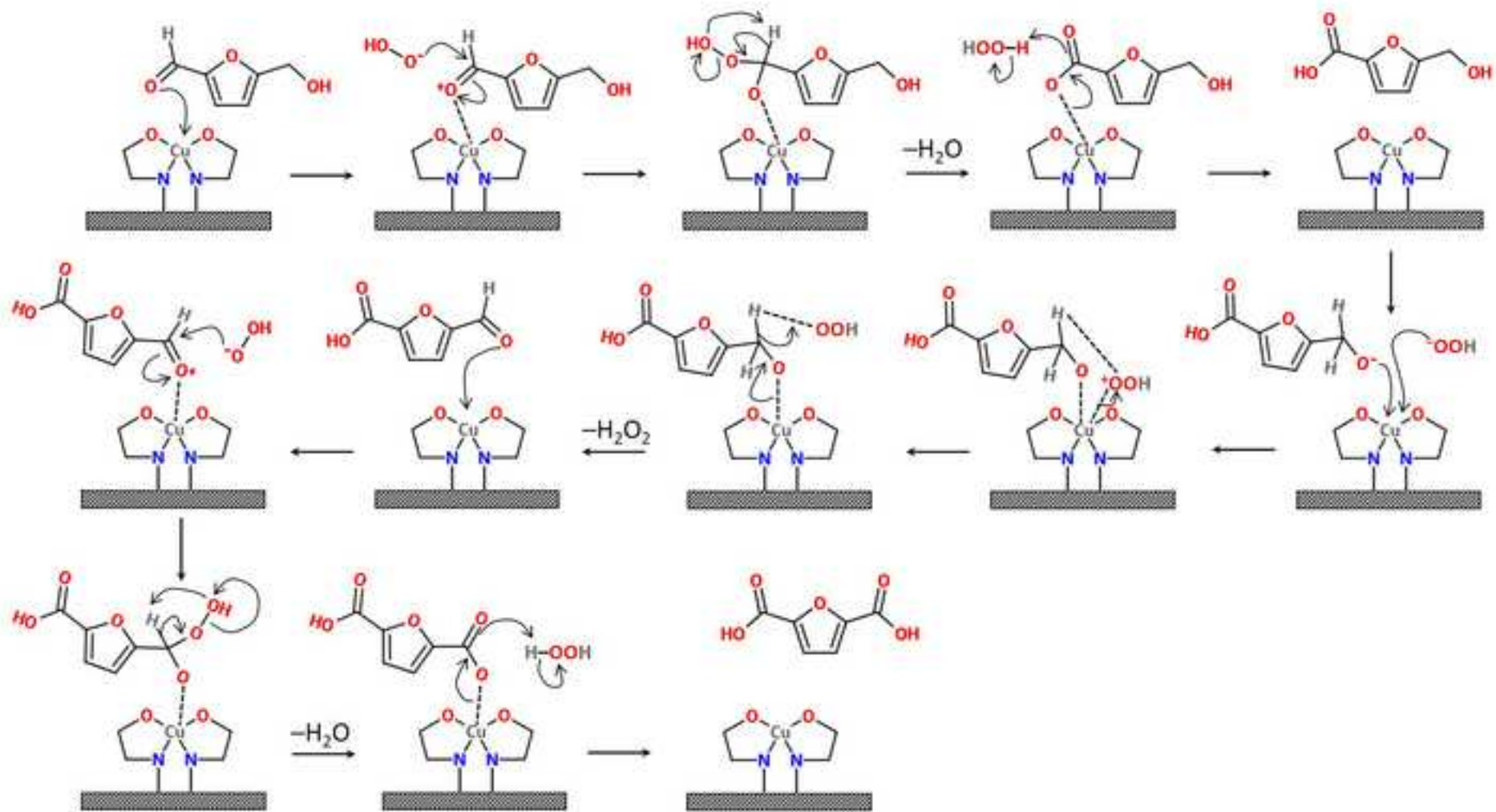
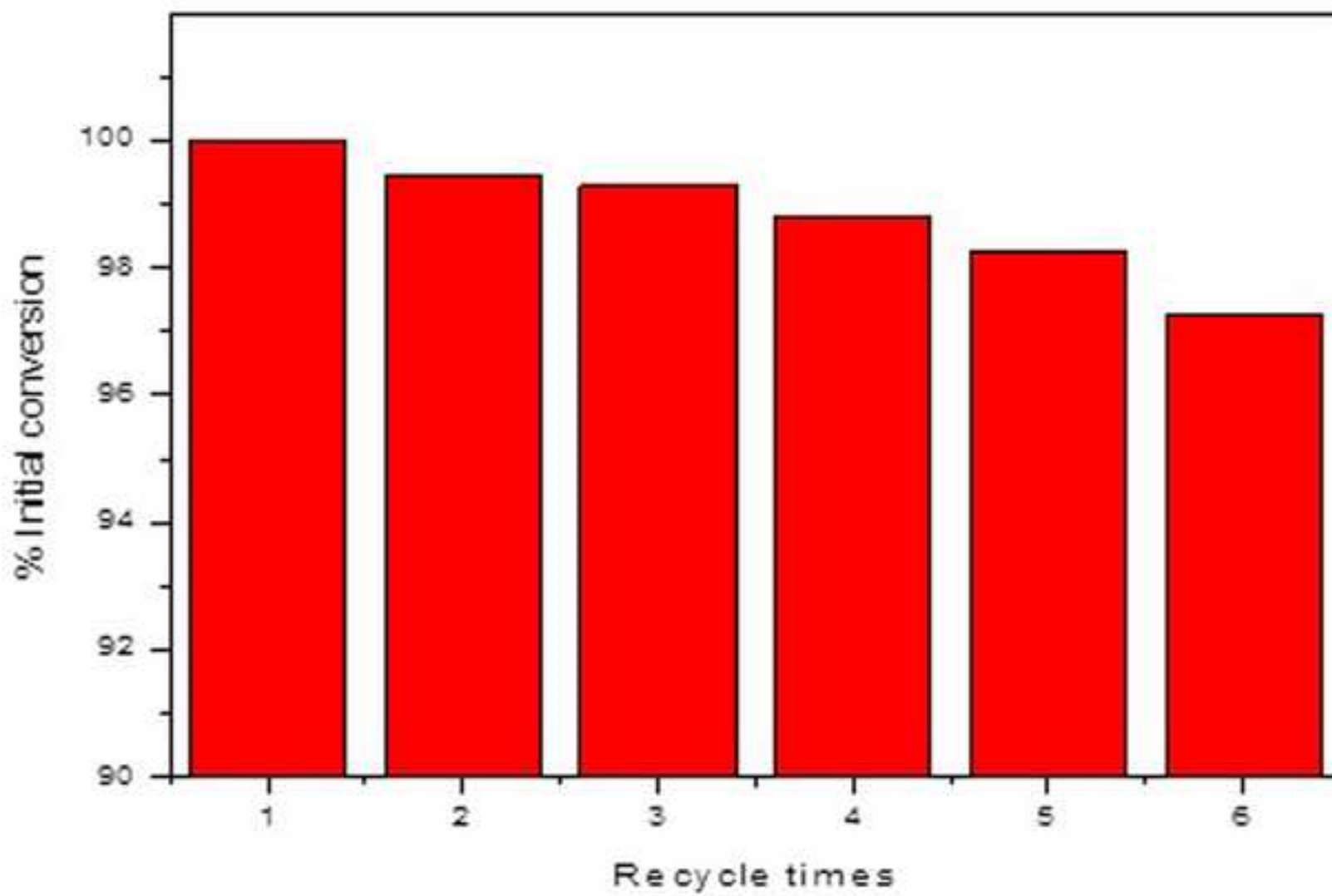


Figure 20



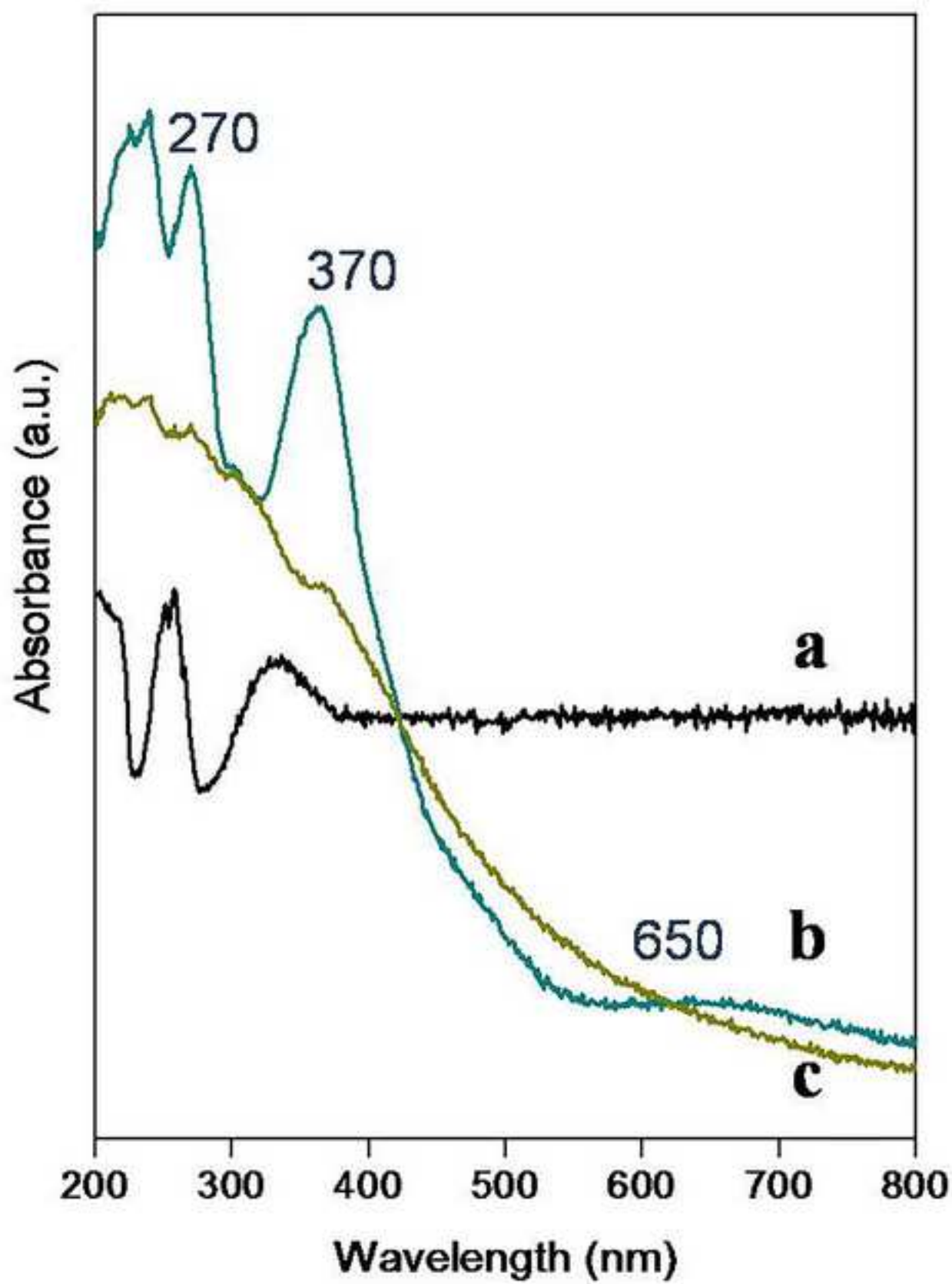


Table 1. Comparative properties of the textural properties of the metal Salen complex catalysts and SBA-15.

Sample	S_{BET}^2 (m ² /g)	% Decrease or S_{BET} with respect of SBA-15	Average D_p (nm)	V_p^3 (cm ³ /g)
SBA-15	583	—	3.81	0.6653
Co salen/SBA-15	311	47	3.81	0.2326
Cu salen/SBA-15	278	52	3.80	0.2009
Fe salen/SBA-15	390	33	3.82	0.2515

Table 2. Kinetic parameters obtained from fit.

k	k_1	k_2	k_3	k_4
(min ⁻¹)				
1.0	1×10^{-2}	2.2×10^{-2}	4.5×10^{-3}	8×10^{-3}

Table 3. Summary of maximum HMF % conversion HMF and % selectivity to identified products at 25 °C.

Catalyst	Activity test		% Selectivity				% Conversion*	
	Oxidant agent	Oxidant agent amount (μL)	DFF	FFCA	FDCA	HMFCa	Identified products	HMF
---	H ₂ O ₂	100	2.05	0.82	3.83	0.7	7.40	40
Co Salen/SBA-15	H ₂ O ₂	100	2.93	1.21	1.63	0.37	6.14	41
Fe Salen/SBA-15	H ₂ O ₂	100	1.93	0.63	4.23	0.62	7.41	>99
Cu Salen/SBA-15	H ₂ O ₂	100	2.42	1.79	5.07	1.05	10.33	>99
	H ₂ O ₂	5	14.39	7.52	0	8.25	30.16	5

- Total conversion at 100 min